

ARTICLE OPEN



Directing negative emotional states through parallel genetically-distinct basolateral amygdala pathways to ventral striatum subregions

Sarah E. Sniffen^{1,2,5}, Sang Eun Ryu^{1,5}, Milayna M. Kokoska¹, Janardhan Bhattarai³, Yingqi Wang³, Ellyse R. Thomas¹, Graylin M. Skates¹, Natalie L. Johnson¹, Andy A. Chavez¹, Sophia R. Iaconis¹, Emma Janke³, Yun-Feng Zhang^{3,4}, Minghong Ma³ and Daniel W. Wesson¹✉

© The Author(s) 2025

Distinct basolateral amygdala (BLA) cell populations influence emotions in manners thought important for anxiety and anxiety disorders. The BLA contains numerous cell types which can broadcast information into structures that may elicit changes in emotional states and behaviors. BLA excitatory neurons can be divided into two main classes, one of which expresses *Ppp1r1b* (encoding protein phosphatase 1 regulatory inhibitor subunit 1B) which is downstream of the genes encoding the D1 and D2 dopamine receptors (*Drd1* and *Drd2* respectively). The role of *Drd1*+ or *Drd2*+ BLA neurons in learned and unlearned emotional responses is unknown. Here, we identified that the *Drd1*+ and *Drd2*+ BLA neuron populations form two parallel pathways for communication with the ventral striatum. These neurons arise from the basal nucleus of the BLA, innervate the entire space of the ventral striatum, and are capable of exciting ventral striatum neurons. Further, through two separate behavioral assays, we found that the *Drd1*+ and *Drd2*+ parallel pathways distinctly influence both learned and unlearned emotional states when they are activated or suppressed and do so depending upon where they synapse in the ventral striatum – with unique contributions of *Drd1*+ and *Drd2*+ circuitry on negative emotional states. Overall, these results contribute to a model whereby parallel, genetically-distinct BLA to ventral striatum circuits inform emotional states in a projection-specific manner.

Molecular Psychiatry (2025) 30:4801–4814; <https://doi.org/10.1038/s41380-025-03075-0>

INTRODUCTION

The ability to evaluate a sensory stimulus and to correctly act upon it is paramount for survival. Abnormal associations of stimuli and/or abnormal actions towards stimuli are hallmark features of psychiatric disorders including anxiety disorders. The basolateral amygdala (BLA) has long been known to support emotional responses [1–3], including to both aversive [4–8] and appetitive stimuli [9–11]. Affording the BLA with this capacity are both its intrinsic plasticity [12, 13] and its projections into ‘downstream’ structures which can directly influence decisions and behavioral outcomes. For instance, the BLA innervates the central nucleus of the amygdala, and this input is necessary for the expression of learned avoidance [14]. Photostimulating central amygdala projecting BLA neurons evokes avoidance, while photoinhibition of the same neurons reduces fear learning [15]. Other projections of the BLA can influence appetitive responses, including stimulation of BLA neurons that project to the ventral striatum’s nucleus accumbens (NAc) [15]. Thus, it is clear that regionally-separable downstream recipients of BLA input are sufficient to direct emotional responses.

There is also an interplay between BLA projection targets and the cell types which comprise those projections in how specific

BLA outputs influence emotion. The genetic identity of BLA neurons is highly diverse and these different cell types appear to be uniquely engaged following emotional responses [16]. A single genetically distinct neuronal population can drive opposing emotional responses if it projects to two brain regions [17] and likewise, two genetically distinct BLA outputs can drive opposing emotional responses if they each project to the same brain region [18]. BLA excitatory neurons are divided into two main genetic classes, which are becoming increasingly understood to have diverse projection targets and functions. These include the *Rspo2* expressing neurons (encoding R-spondin 2) which can drive aversive behaviors, and the *Ppp1r1b* expressing neurons (encoding protein phosphatase 1 regulatory inhibitor subunit 1B) which appear to support appetitive behaviors [19]. BLA neurons distinguished by the expression of the transcription factor *RSPO2* are also labeled by *Fezf2* (encoding the transcription factor zinc-finger 2) [17] and project to the NAc and also its neighboring ventral striatum subregion, the tubular striatum (TuS, also known as the olfactory tubercle) [20]. Activation of *Fezf2* neurons innervating the NAc drives aversive states, and contrastingly, activation of *Fezf2* neurons innervating the TuS increases

¹Department of Pharmacology and Therapeutics, University of Florida College of Medicine, Florida Chemical Senses Institute, Gainesville, FL 32610, USA. ²Department of Neuroscience, University of Florida College of Medicine, Gainesville, FL 32610, USA. ³Department of Neuroscience, Perelman School of Medicine, University of Pennsylvania, Philadelphia, PA 19104, USA. ⁴State Key Laboratory of Integrated Management of Pest Insects and Rodents, Institute of Zoology, Chinese Academy of Sciences, Beijing, China. ⁵These authors contributed equally: Sarah E. Sniffen, Sang Eun Ryu. ✉email: danielwesson@ufl.edu

Received: 19 June 2024 Revised: 5 May 2025 Accepted: 3 June 2025
Published online: 13 June 2025

appetitive states. Together, these findings indicate that neither the downstream target nor the genetic identity alone sufficiently explain how the BLA broadcasts emotional information. Instead, where this information goes *and* who within the BLA sends it are *both* critical for regulating emotional states. Given that *Rspo2/Fezf2* + BLA neurons support both appetitive and aversive states depending upon their downstream targeting, we sought to answer the question of whether the *Ppp1r1b* + BLA neuron population also contributes to aversive states, and if they do so depending upon their regional innervation within the NAc and TuS.

Ppp1r1b (also known as DARPP-32, dopamine- and cAMP-regulated neuronal phosphoprotein) is a phosphoprotein regulated by both D1 and D2 dopamine receptors [21–23], which are encoded for by the *Drd1* and *Drd2* genes, respectively [24]. Dopamine within the BLA is necessary for fear learning [25]. We know that *Drd1* + neurons in the BLA contribute to memory [26]. While the role of *Drd2* + neurons in the BLA is not understood, prior pharmacological work has indicated a role for the D2 receptor in emotional responses [27–29]. Overall, the respective contributions of *Drd1* + and *Drd2* + BLA neurons in regulating emotional states are unknown. Moreover, it is unknown if, like the *Fezf2* neurons, the influence of *Drd1* + and *Drd2* + BLA neurons depends upon their projection targets. Here, using a combination of viral tracing, ex vivo brain slice recordings, chemo- and optogenetics, and behavior, we identified that the *Drd1* + and *Drd2* + BLA neuron populations form two parallel pathways wherein each innervate both the NAc and the TuS for the modulation of negative emotional states depending upon which ventral striatum subregion they innervate. Overall, these results contribute to a model whereby parallel, genetically-distinct, BLA to ventral striatum circuits inform emotional states in a projection-specific manner and altogether expand our appreciation for how the BLA regulates emotions.

MATERIALS AND METHODS

Ethics approval

All experimental procedures were conducted at the University of Florida or the University of Pennsylvania in accordance with the relevant guidelines from the Guide for the Care and Use of Laboratory Animals. Vertebrate animal procedures were approved and followed the guidelines and regulations set by each institution's respective Institutional Animal Care and Use Committees (protocol 202300000126 at Univ of Florida and protocol 803920 at Univ of Pennsylvania).

Animals

Adult male and female mice, 2–5 months of age, were housed in a temperature-controlled vivarium on a 12:12 h (hr) light/dark cycle with *ad libitum* access to food and water, except during behavioral testing. All behavioral testing occurred during the light cycle. Mice that only underwent viral injections were group housed (≤ 5 mice/cage) and mice with chronic implants were single housed following surgery.

Mouse lines included the following transgenic lines which were maintained on a C57BL/6J background (strain #000664; RRID:IMSR_JAX:000664, The Jackson Laboratory) and were bred in house within a University of Florida vivarium. *Drd1*-Cre (B6.FVB(Cg)-Tg(*Drd1*-cre)EY262G-sat/Mmucd, RRID:MMRRC_030989-UCD), *Drd2*-Cre (B6.FVB(Cg)-Tg(*Drd2*-cre)ER44Gsat/Mmucd, RRID:MMRRC_032108-UCD), and *A2a*-Cre (B6.FVB(Cg)-Tg(*Adora2a*-cre)JG139Gsat/Mmucd, RRID:MMRRC_036158-UCD) mice were obtained from the UC Davis Mutant Mouse Regional Resource Center (MMRRC) [30]. *Drd1*-tdTomato/*Drd2*-GFP double transgenic mice originate from that described previously [31]. Ai9 tdTomato Cre reporter mice (B6.Cg-Gt(ROSA)26Sor^{tm9(CAG-tdTomato)Hze}/J; RRID:IMSR_JAX:007909, [32]) were obtained from the Jackson Laboratory.

The sample size of animals in each experiment was selected based upon our prior experiences which yielded statistically robust outcomes with similar sample sizes (*viz.*, no *a priori* statistical power was calculated). Data from animals with implants not appropriately targeted to their region intended (e.g., BLA, NAc, TuS), or with viral expression extending outside of

those regions, were eliminated from analyses and are not reported herein. For all experiments, every attempt was made to pseudorandomize the experimental groups so that as many groups as possible would be included in any given replication. While for the behavioral experiments the experimenter was not blind due to the nature of the experiments (e.g., required pre-treatment with drugs, etc), post-processing and handling of data were both performed using semi-automated methods (see below).

Viral vectors

rgAAV.hSyn.H1eGFP-Cre.WPRE.SV40 (Addgene #105540-AAVrg, 7×10^{12} vg/ml), AAV.Ef1a.DIO.Synaptophysin.mRuby and AAV.Ef1a.FLEX.Synaptophysin.GFP (both generous gifts from Dr Marc Fuccillo, University of Pennsylvania) [33], and AAV.hSyn.FLEX.mGFP-2A-Synaptophysin.mRuby (Addgene #71760-AAV1, 9.8×10^{12} vg/ml) were used for tracing. AAV.Ef1a-DIO.hChR2(E123T/T159C)-EYFP (Addgene #35509-AAV5, 1×10^{12} vg/ml vg/ml) was used for patch-clamp recording and for optogenetic stimulation during the optogenetic real-time place preference/avoidance task. AAV.Ef1a.DIO.EYFP (Addgene #27056-AAV5, 1×10^{12} vg/ml) was used as a control virus for the optogenetic real-time place preference/avoidance task. rgAAV.hSyn.DIO.hM4D(Gi)-mCherry (Addgene #44362-AAVrg, 1.2×10^{13} vg/ml) and rgAAV.hSyn.DIO.mCherry (50459-AAVrg, 1.8×10^{13} vg/ml) were used for chemogenetic inhibition. Both the rgAAV.hSyn.DIO.mCherry and rgAAV.hSyn.DIO.GFP (Addgene #50457-AAVrg, 7×10^{12} vg/ml) were used for retrograde tracing of BLA neurons to assess possible collateralization of inputs to ventral striatum.

Surgical procedures

For all surgical procedures, mice were anesthetized with 2–4% isoflurane (IsoFlo, Patterson Veterinary, Greeley, CO) in 1 L/min (min) O₂, and head fixed in a stereotaxic apparatus while their body temperature was maintained using a 38 °C water bath heating pad. The scalp was shaved and cleaned with betadine and 70% ethanol. Following subcutaneous (s.c.) administration of Meloxicam (20 mg/kg) analgesia and local administration of the anesthetic lidocaine (lidocaine, 3 mg/kg, s.c., Patterson Veterinary) to the scalp, a small midline cranial incision was made.

For viral injections, craniotomies were made above the target regions. A pulled glass micropipette containing the AAV was slowly inserted for injection. For TuS injections, 50 nl of viral solution was injected bilaterally at the following coordinates: anteroposterior (AP) + 1.4 mm bregma, medio-lateral (ML) ± 1.2 mm lateral midline, dorsoventral (DV) -4.85 mm from the brain surface for DREADD based behaviors, or 50 nl of viral solution was delivered unilaterally for tracing experiments. For NAc injections, 100 nl of viral solution was delivered bilaterally (AP 1.5 mm, ML ± 1.0 mm, DV -3.75 mm) for behavioral experiments, or 50 nl of viral solution was delivered unilaterally for tracing experiments. For BLA injections, 100 nl of viral solution was delivered either unilaterally into the right hemisphere (AP -1.6 mm, ML + 3.25 mm, DV -4.25 mm) for Opto-RTPP/A and brain slice electrophysiology experiments, or bilaterally (AP -1.6 mm, ML ± 3.25 mm, DV -4.25 mm) for tracing experiments. All injections were performed at a rate of 2 nl/s (s), with 20–40 s intervals using a Nanoject III (Drummond Scientific). Following injection, at least 5 min went by before slowly withdrawing the pipette from the brain. Craniotomies were then sealed with dental wax and the incision was closed with wound clips.

For cannula implantation, the skull was scrubbed with 3% H₂O₂ and covered with a thin layer of cyanoacrylate glue (Vetbond, 3M). Bilateral craniotomies were drilled over the BLA and 26-gauge(G) guide cannulae (#C315GMN/SPC, P1 Technologies) extending 3.5 mm below pedestal were implanted at the coordinates AP -1.3 mm, ML ± 3.2 mm. Cannulae were then lowered into the brain and secured to the skull with a small amount of Vetbond followed by dental cement, and dust caps with a 3.5 mm projection wire (C315DCMN/SPC, P1 Technologies) were inserted.

For optical fiber implantation, following skull preparation for implantation as above, a craniotomy was made and drilled above the ventral striatum on the right hemisphere. Fibers (300 μ m core diameter, 0.39NA, cut to 6.0 mm length) for optogenetic stimulation were lowered into the NAc (AP 1.4 mm, ML 1.0 mm, DV -3.85 mm) or the TuS (AP 1.5 mm, ML 1.2 mm, DV -4.9 mm). The fiber was secured with Vetbond followed by dental cement as described for the cannulae implantation.

Following surgery, mice were allowed to recover on a heating pad until ambulatory and were given immediate *ad libitum* access to food and water. Meloxicam analgesic (20 mg/kg, s.c.) was administered for at least 3 days following surgery. Mice with indwelling cranial implants were single housed and given 7–14 days after surgery to recover before being acclimated to behavioral procedures.

Histology

Immunohistochemistry. Mice were anesthetized with Fatalplus (150 mg/kg; Vortech Pharmaceutical Ltd, Dearborn, MI) and transcardially perfused with cold 0.9% NaCl (Physiological Saline), followed by cold 10% phosphate buffered formalin (#SF100-4, Thermo Fisher Scientific) for fixation. Brains were collected and further fixed and cryoprotected in a 30% sucrose/10% formalin solution for 72 hr at 4 °C. Serial 40 µm thick coronal sections were collected using a sliding microtome (Leica) and stored at 4 °C in a solution of Tris-buffered saline (TBS; 0.242% Tris base, 2.924% sodium chloride, pH = 7.4 ± 0.2) with 0.03% sodium azide.

Sections from *Drd1*- or *Drd2*-Cre mice injected with Cre-dependent retrograde mCherry AAV underwent antigen retrieval in citrate buffer (pH 6.0) for 30 mins at 80 °C. Sections from *Drd1*-Cre;Ai9, *Drd2*-Cre;Ai9, or *A2a*-Cre;Ai9 mice were selected to investigate recombination efficiency but did not undergo antigen retrieval. After being rinsed with TBS and diluting buffer (2% bovine serum albumin (Sigma Aldrich), 0.9% sodium chloride (Sigma Aldrich), 0.4% Triton-X 100 (Sigma Aldrich), and 1% normal goat serum (Sigma Aldrich) in TBS), samples were blocked in 20% normal donkey serum solution, then incubated in the primary antibody overnight at 4 °C. Sections were then incubated in the secondary antibody at room temperature and washed with TBS prior to slide-mounting with either DAPI Fluoromount-G® mounting medium (SouthernBiotech, catalog #0100-20). Primary antibodies included rabbit anti-DsRed (Takara Bio, catalog #632496, 1:1000), chicken anti-NeuN/FOX3 (EnCor, catalog #PCPA-FOX3, 1:1000), and mouse anti-Cre Recombinase (Millipore-Sigma, cat#MAB3120, 1:1000). Secondary antibodies included goat anti-chicken Alexa Fluor 488 (Invitrogen, cat#A11039), goat anti-rabbit Alexa Fluor 680 (Invitrogen, cat#A21109), and donkey anti-mouse Alexa-Fluor 488 (Invitrogen, cat#A21202), all at a 1:1000 dilution.

Imaging and quantification. Brain regions were identified using the mouse brain atlas [34]. Images were acquired using a Nikon Eclipse Ti2e fluorescent microscope. For quantification of the number of *Drd1*+ and *Drd2*+ NAc and TuS projecting BLA neurons, three mice of each genotype (*Drd1*-Cre or *Drd2*-Cre) received an injection in either the NAc or the TuS. From these mice, at least three BLA sections were acquired and imaged from −1.10 mm to −2.10 mm posterior to Bregma. For quantification of the number of Cre+ neurons in the BLA of *Drd1*-Cre;Ai9, *Drd2*-Cre;Ai9, or *A2a*-Cre;Ai9 mice, at least five BLA sections from three mice of each genotype were acquired spanning the same range. Images were acquired at 20x magnification across both hemispheres and Z-stacked every 4 µm. For quantification, regions of interest (ROIs) were drawn around the areas of interest (LA, BA). Images were preprocessed to remove background and to enhance local contrast, a rolling ball algorithm was applied to remove background, and images underwent Gaussian smoothing and Laplace sharpening. A semi-automated thresholding and counting algorithm created within NIS elements (Nikon) software was used to identify cells within selected ROIs, allowing for unbiased estimation of cell numbers. Cells were identified based on fluorescence intensity (via threshold) and diameter.

For quantification of *Drd1*+ and *A2a*+BLA to ventral striatum synaptophysin puncta within the ventral striatum, at least three sections from three mice of each genotype were acquired spanning from 1.7–0.6 mm anterior to Bregma. Images were acquired at 20x magnification for the hemisphere ipsilateral to the injection site, and Z-stacked every 0.9 µm. For quantification, ROIs were drawn around the areas of interest (TuS, NAcC, NAcSh, PCx). Images were preprocessed to remove the average background. A semi-automated thresholding and counting algorithm created within NIS elements software was used to identify fluorescent puncta within selected ROIs, allowing for unbiased estimation of the number of fluorescent puncta. Puncta were identified based on fluorescence intensity (via threshold) and diameter.

Brain slice electrophysiology. Whole-cell patch-clamp recordings were performed in ex vivo brain slices from *Drd1*-Cre;Ai9 or *A2a*-Cre;Ai9 mice, in which tdTomato expression was directed within cells expressing either DRD1 or DRD2, respectively. A Cre dependent AAV encoding for ChR2 (AAV5-Ef1a-DIO hChR2(E123T/T159C)-EYFP) was injected bilaterally into the BLA of *Drd1*-Cre;Ai9 or *A2a*-Cre;Ai9 mice, 2–3 months of age. After waiting a minimum of one month to allow for ample AAV expression, acute brain slices were prepared as follows.

Mice were deeply anesthetized with intraperitoneal injection of ketamine-xylazine (200–15 mg/kg body weight) and decapitated. The cranium was dissected and the brain was immediately removed and placed in ice-cold HEPES buffered cutting solution containing (in mM): 92 N-methyl-D-glucamine, 2.5 KCl, 1.2 NaH₂PO₄, 30 NaHCO₃, 20 HEPES, 25

glucose, 5 sodium L-ascorbate, 2 thiourea, 3 sodium pyruvate, 10 MgSO₄ and 0.5 CaCl₂ (osmolality ~300 mOsm and pH ~7.4, bubbled with 95% O₂ and 5% CO₂). Coronal brain slice (180–200 µm) containing the OT were cut using a Leica VT 1200S vibratome. Brain slices were incubated in oxygenated artificial cerebrospinal fluid (ACSF) containing (in mM): 126 NaCl, 2.5 KCl, 2.4 CaCl₂, 1.2 MgSO₄, 1.4 NaH₂PO₄, 11 glucose, 25 NaHCO₃ and 0.6 sodium L-ascorbate (osmolality ~300 mOsm and pH ~7.4, bubbled with 95% O₂ and 5% CO₂) for 1 hr at 31 °C and at room temperature thereafter. Slices were transferred to the recording chamber for whole-cell patch-clamp recordings and continuously perfused with oxygenated ACSF. 4-Aminopyridine (4-AP; 200 µM) was added to enhance optically evoked synaptic release in ChR2+ axonal terminals. Fluorescent DRD1-/A2A-tdTomato+ cells in the TuS were visualized with a 40X water-immersion objective under an Olympus BX51WI upright microscope equipped with epifluorescence. Electrophysiological recordings were controlled by an EPC-10 amplifier combined with Pulse Software (HEKA Electronic) and analyzed using pulse and Clampfit (Axon instruments). Whole-cell patch-clamp recordings were made in both current and voltage-clamp mode. Patch pipettes were pulled from thin-wall borosilicate glass-capillary tubing (WPI, Sarasota, FL, USA) on a Flaming/Brown puller (P-97; Sutter Instruments Co., Novato, CA, USA). The tip resistance of the electrode was 5–8 MΩ. The pipette solution contained the following (in mM): 120 K-gluconate, 10 NaCl, 1 CaCl₂, 10 EGTA, 10 HEPES, 5 Mg-ATP, 0.5 Na-GTP, and 10 phosphocreatine.

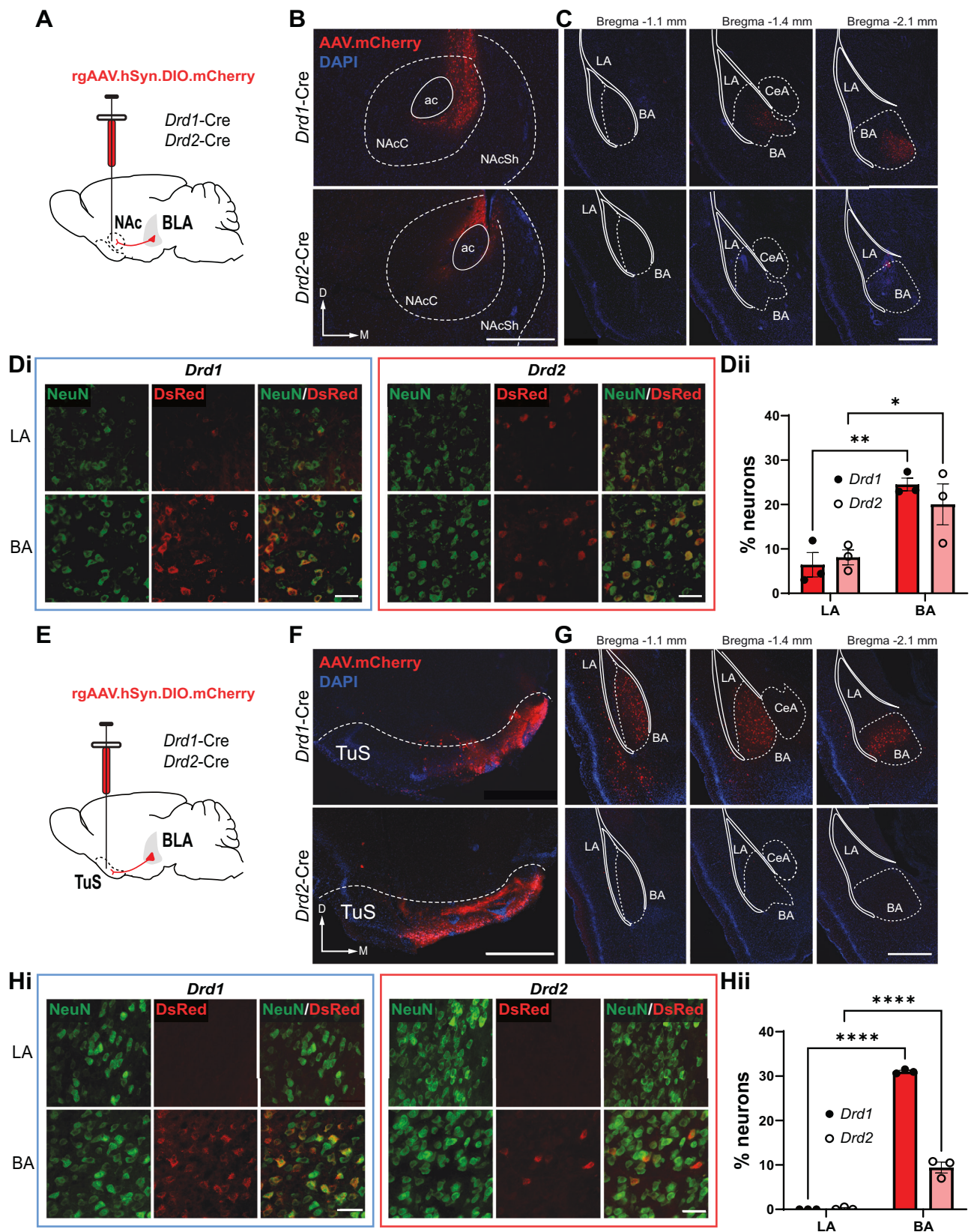
To activate ChR2 in the TuS slices, blue light (pE-300ultra, CoolLED, ~25 mW) was delivered through the same 40X objective. Pharmacological reagents including tetrodotoxin (TTX) citrate (Abcam), 6-cyano-7-nitroquinoxaline-2,3-dione (CNQX), D,L-2-amino-5-phosphonopentanoic acid (AP5), and 4-Aminopyridine (4-AP) (Sigma-Aldrich) were bath perfused during recording.

in vivo DREADD-based chemogenetic inhibition. For DREADD-based chemogenetic inhibition of Gi coupled inhibitory DREADD receptor (hM4Di) expressing neurons, *Drd1*+ and *Drd2*+ mice were injected with rgAAV.hSyn.DIO.hM4D(Gi)-mCherry (1.2×10^{13} vg/ml, 100 nl/hemisphere in NAc, 50 nl/hemisphere in TuS, catalog #44362-AAVrg, Addgene) or rgAAV.hSyn.DIO.mCherry (1.8×10^{13} vg/ml, 100 nl/hemisphere in NAc, 50 nl/hemisphere in TuS, catalog #50459-AAVrg, Addgene) as control. All mice were implanted 1–2 weeks later with bilateral intracranial guide cannulae (Protech International, Inc, catalog #8IC315GMNSPC, 26ga) extending 3.5 mm beyond the pedestal, for direct administration of either the DREADD ligand J60 [35] or vehicle into the BLA. Dust caps without a projection were (Protech International, Inc, catalog #8IC315DCMNSP) were inserted immediately following surgery, and mice were given 1–2 weeks to recover.

Prior to behavior, mice underwent 2 days of handling in which the dummy cannulae were removed and replaced. On the habituation behavior day, mice received a “mock” infusion, wherein the internal cannulae (Protech International, Inc, catalog #8IC315MNSPC, 5.75 mm projection, 33ga) connected to tubing from a 1 µL Hamilton Syringe (Hamilton, catalog #86211) were inserted into the guide cannulae, and the Harvard Apparatus 22 Syringe Pump (catalog #PY2 55–2222) was turned on for 2 min to simulate the noise of the infusion. This mock infusion occurred 30 min prior to being placed in the plethysmograph for the Pavlovian fear learning behavioral paradigm. On the learning day (Day 2) of the Pavlovian fear learning paradigm, mice were once again tethered to the Hamilton syringe, but this time received an infusion of 100 nL of either 10 nM J60 or vehicle at a rate of 50 nL/min, 30 min prior to the start of the behavioral task.

Behavioral tasks

Odor-shock pavlovian fear learning. We used a whole-body plethysmography chamber (Data Sciences International, St. Paul, MN) that was adapted for the infusion of a neutral odor and the administration of a mild foot shock for an odor-shock Pavlovian fear learning test, as originally developed for use in rats [36]. We constructed an air-dilution olfactometer [37, 38] and used custom code in Synapse (Tucker Davis Technologies) to control the delivery of an otherwise neutral odor, isopentyl acetate (1 torr in liquid state; Sigma Aldrich), at a flow rate of 1 L/min (20 s) which co-terminated with the presentation of a mild foot shock (0.5 mA for 1 s). Respiratory transients were detected using a Data Sciences pressure transducer, gain amplified 100× (Cygnus Technology Inc), and digitized (0.1–20 Hz) at 300 Hz in Synapse. Positive pressure of clean room air was continuously applied to the chamber using a stable-output air pump (Tetra



Whisper). Following each stimulus trial, odor-vaporized air was exhausted from the plethysmograph through an outlet at the chamber's ceiling.

Mice were acclimated to handling in the behavioral room for two days prior to entering the plethysmograph. Mice were then acclimated to the

plethysmograph by undergoing a session in which no odors or shock were delivered, but the associated sounds were present (Supplementary Fig. 5). Twenty-four hr later on the acquisition day, mice were allowed to acclimate to the plethysmograph for a 4 min period and were then

Fig. 1 **Ventral striatum projecting BLA neurons arise from the BA and are comprised of *Drd1*⁺ and *Drd2*⁺ neurons.** **A** Schematic of approach for identifying BLA *Drd1*⁺ and *Drd2*⁺ inputs to the NAc. **B** Example of a NAc injection in *Drd1*-Cre (top) and *Drd2*-Cre (bottom) mice (ac = anterior commissure, NAcC & NAcSh = nucleus accumbens core & shell, respectively), and **C** example images of NAc projecting *Drd1*⁺ (top) or *Drd2*⁺ (bottom) neurons along the anterior-posterior axis of the BLA. Scale bars = 500 μ m. **Di** Anti-NeuN and anti-DsRed immunofluorescence images to identify the size of the NAc projecting BLA neural population. Scale bars = 40 μ m. **Dii** Quantification of the *Drd1* (** p < 0.01, n = 3, 2/1/sex) or *Drd2* (* p < 0.05, n = 3, 2/1/sex) expressing BLA cells along the entire AP axis that project to the NAc (Two-way ANOVA, ROI main effect $F(1,8)$ = 26.65, p = 0.001). **E** Schematic of approach for identifying BLA *Drd1*⁺ and *Drd2*⁺ inputs to the TuS (TuS = tubular striatum). **F** Example of a TuS injection in *Drd1*-Cre (top) and *Drd2*-Cre (bottom) mice, and **G** example images of TuS projecting *Drd1*⁺ (top) or *Drd2*⁺ (bottom) neurons along the anterior-posterior axis of the BLA. Scale bars = 500 μ m. **Hi** Anti-NeuN and anti-DsRed immunofluorescence images to identify the size of the NAc projecting BLA neural population. Scale bars = 40 μ m. **Hii** Quantification of the *Drd1* (**** p < 0.0001, n = 3, 2/1/sex) or *Drd2* (**** p < 0.0001, n = 3, 2/1/sex) expressing TuS projecting BLA cells along the entire AP axis (Two-way ANOVA, ROI main effect $F(1,8)$ = 295.3, p < 0.001). Mean \pm SEM.

presented with 10 trials of 20 s odor delivery co-terminating with an odor-paired 1 s foot shock (0.5 mA) with an inter-trial interval (ITI) of 180 s. For the unpaired fear conditioning task, the foot shock was presented pseudorandomly in the ITI (90 s after the foot shock). For the odor only control mice, the 10 trials consisted of only 20 s odor delivery without the administration of the foot shock. The shocked mice received no odor delivery during the trials but received a foot shock either at the end of the trial (trial shock group) or pseudorandomly in the ITI (ITI-shock group). Mice were then returned to their home cage. Twenty-four hr later on the retrieval day, the odor was presented for 10 trials without the foot shock for all groups receiving odor (paired, unpaired, and odor only groups). Mice who did not previously receive the odor underwent the 10 trials without odor delivery or foot shock. Mobility behavior was recorded throughout the entire fear conditioning task using two digital cameras (Microsoft, 10 Hz frame rate) and was scored in 0.4 s bins during the 19 s of odor presentation prior to shock using ezTrack [39] to identify periods of physical immobility. Respiration digitized from the pressure transducer was imported into MATLAB, and a MATLAB script was used to calculate fast-fourier transform (FFT) power spectra of the respiratory signal during odor (excluding the 1 s when the shock co-occurred) as compared to pre-odor (see Supplementary Fig. 5).

Optogenetic real-time place preference or aversion test (Opto-RTPP/A). Mice were gently handled and acclimated to the behavior room the day prior to the opto-RTPP/A test. Prior to starting the opto-RTPP/A test, mice were gently scruffed, the dust cap was removed, and the mice were tethered to a 400 μ m, 0.57NA fiber (Thorlabs, catalog #M58L01) and placed in a 15.24 \times 40.64 \times 27.94 cm (length \times width \times height) apparatus divided into three chambers. This fiber was connected to an LED (Doric, 465 nm) through a rotary joint connected to a 400 μ m, 0.39NA patch cable. Mice were placed in the center of a three-chamber apparatus and allowed to explore for 30 min. An infrared video camera was placed above the chamber to record activity of the mouse in each chamber (12 Hz frame rate). When mice entered into one of the three chambers, and subsequently broke the infrared beam path, light stimulation (465 nm, 15 ms pulse width, 40 Hz) was initiated and continuously delivered until mice left the chamber and ceased breaking the infrared beams (controlled by an Arduino). At the end of the 30 min, mice were gently restrained and the tether was removed. Mice were then returned to their home cage. The mice were euthanized and perfused the same day, and brains were collected for histological verification of virus injection and optic fiber placement. Analyses were performed in ezTrack [39] to quantify the time spent in each chamber and to generate maps of physical space for illustration purposes.

Data analysis. Data were analyzed for statistical significance in GraphPad Prism. All data are reported as mean \pm SEM unless otherwise noted. Specific tests used can be found in the Results sections or the figure legends. All tests met the assumptions of the test (e.g., were normally distributed, etc.) and variances between groups comparable. All t -tests were paired. When possible, experimenters handling the data were blinded to treatment conditions and all post-processing and analyses of data handled through semi-automated methods when possible.

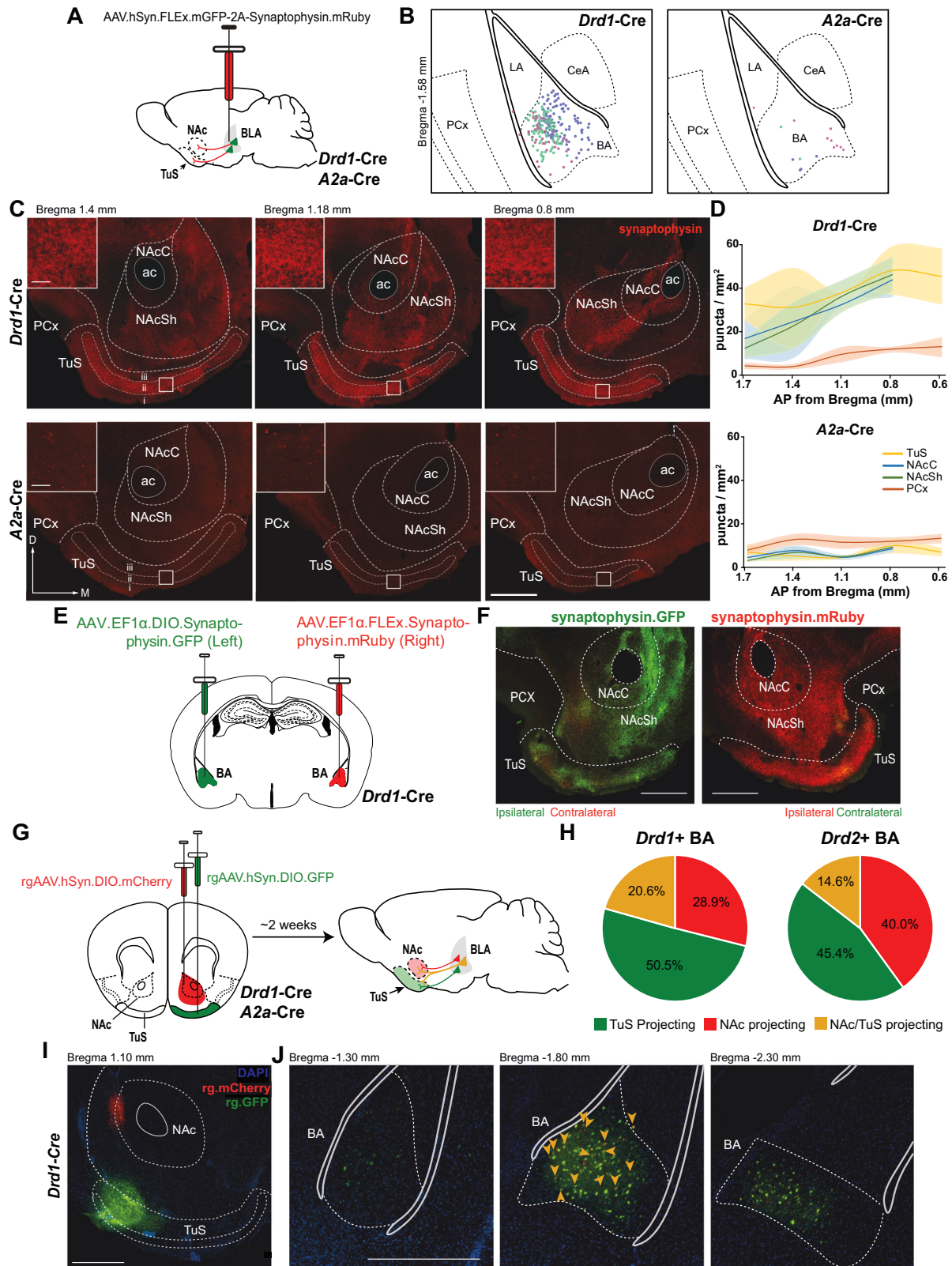
RESULTS

***Drd1*⁺ and *Drd2*⁺ BLA neurons innervate the ventral striatum** While we know that the BLA possesses *Drd2*⁺ and *Drd1*⁺ neurons, with more of the latter [40], we sought to determine if BLA *Drd1*⁺

and *Drd2*⁺ neurons form a circuit with ventral striatum neurons. We injected a Cre-dependent retrograde (rg) AAV expressing mCherry, rgAAV.hSyn.DIO.mCherry, into either the NAc or the TuS of *Drd1*-Cre and *Drd2*-Cre mice [41] (Fig. 1A, B & E, F) and later inspected the BLA for mCherry⁺ neurons. mCherry⁺ cells in both groups of mice were found in the BLA in both *Drd1*- and *Drd2*-Cre mice (Fig. 1C & G), indicating that these neurons indeed project to the ventral striatum. mCherry⁺ cells were found throughout the entire anterior-posterior extent of the BLA (Fig. 1C & G). In contrast to the lateral amygdala (LA), which was largely void of mCherry⁺ cells, the basal nucleus of the amygdala (BA) displayed dense mCherry⁺ cells (Fig. 1C & G). This organization was observed even when similarly injecting either the NAc or TuS of Ai9.tdTomato Cre-reporter mice [32] with rgAAV.hSyn.H1.eGFP-Cre.WPRE.SV40, suggesting that the BA is a major conduit of ventral striatum input regardless of cell type (Supplementary Fig. 1A–C & D–F). No reciprocal connection from ventral striatum to the BLA was found, however (Supplementary Fig. 1G–I).

To quantify the spatial distribution and to identify the size of the population of *Drd1*⁺ and *Drd2*⁺ BLA neurons innervating both the NAc and TuS, sections were immunolabeled for both NeuN, to measure the total number of neurons, and the red fluorescent protein DsRed, to amplify the mCherry fluorescent signal (Fig. 1Di & Hi). This revealed that indeed the vast majority of ventral striatum projecting *Drd1*⁺ and *Drd2*⁺ neurons arise from the BA (Fig. 1Dii, NAc: *Drd1*⁺ MLSD = |BA-LA| = 18.07, p = 0.002, *Drd2*⁺ MLSD = |BA-LA| = 11.95, p = 0.019; Fig. 1Hii, TuS: *Drd1*⁺ MLSD = |BA-LA| = 31.0, p < 0.001, *Drd2*⁺ MLSD = |BA-LA| = 9.24, p < 0.001; MLSD = mean least square difference). Importantly, we confirmed in *Drd1*-RFP;*Drd2*-GFP double transgenic mice [31] that there is minimal co-expression of DRD1 and DRD2 in BLA and ventral striatum cells (Supplementary Fig. 2A & B).

Where throughout the ventral striatum do BLA neurons innervate? To answer this, we injected *Drd1*-Cre and *Adora2a* (*A2a*)-Cre mice into the BLA with an AAV encoding a synaptophysin-mRuby fusion protein (AAV.hSyn.FLEX.mGFP-2A-Synaptophysin-mRuby) [33] (Fig. 2A). *A2a*-Cre mice were chosen for all anterograde AAV-based experiments to attempt to achieve optimal presynaptic expression in *Drd2*⁺ neurons, since both 1) *A2a* is found downstream of the D2 dopamine receptor in *Drd2*⁺ neurons and 2) *A2a* is enriched in the presynaptic terminals of striatal projection neurons [42]. This resulted in GFP⁺ neurons in the BLA to confirm the injection-site (Fig. 2B) and mRuby⁺ puncta, indicative of BLA *Drd1*⁺ or *A2a*⁺ neuronal synapses, throughout both the NAc and TuS (Fig. 2C). mRuby⁺ puncta were highly visible in *Drd1*⁺ neurons in comparison to *A2a*⁺ neurons (Fig. 2C & D). The mRuby⁺ puncta spanned the entire medial-lateral and anterior-posterior extents of the TuS and were especially prominent in layer 2 (Fig. 2C), which is the densest cell layer. mRuby⁺ puncta were also observed throughout the medial-lateral and anterior-posterior extents of the NAc, with comparable amounts in both the NAc core and shell (Fig. 2D, *Drd1*⁺ MLSD = |NAcC-NAcSh| = 0.035, p > 0.999, *A2a*⁺ MLSD = |NAcC-NAcSh| = 0.241, p > 0.999). It is notable, given its roles in associative learning including fear learning [43, 44], that the



ventral striatum receives more BLA *Drd1+* and less *A2a+* neuronal input than the neighboring piriform cortex (Fig. 2D, *Drd1+* : $F(1,16) = 30.8$, $p < 0.001$; *A2a+* : $F(1,14) = 10.6$, $p = 0.006$).

Next, we asked if the same BLA neurons which innervate the TuS are also those which innervate the NAc and vice versa. We

injected rgAAV.hSyn.DIO.GFP into the TuS and rgAAV.hSyn.DIO.mCherry into the NAc of either *Drd1-Cre* or *A2a-Cre* mice and then inspected the BLA for GFP and mCherry co-expressing cells (Fig. 2G). As shown in Fig. 2H approximately 50% of the ventral striatum projecting *Drd1+* BLA neurons project to the TuS, ~29%

Fig. 2 *Drd1*⁺ and *Drd2*⁺ BLA neurons innervate the entire span of the ventral striatum. **A** Schematic of approach for identifying BLA *Drd1*⁺ and *Drd2*⁺ synaptic innervation of the ventral striatum. **B** Maps of BLA injection sites for *Drd1*-Cre (left) and *A2a*-Cre mice (right), where each color represents individual mice. **C** Representative images showing direct innervation of BLA neurons into the ventral striatum in both *Drd1*- and *A2a*-Cre mice. Inset locations denoted by square white box, inset scale bar = 10 μ m. **D** Quantification of synaptophysin puncta in *Drd1*-Cre ($n = 3$, 2/1/sex) and *A2a*-Cre ($n = 3$, 2/1/sex) mice. Mean \pm SEM. **E** Approach for defining whether, and if so, BLA neurons send contralateral projections to the ventral striatum using an AAV encoding synaptophysin. GFP in the BLA in one hemisphere and synaptophysin.mRuby in the BLA in the opposite hemisphere. **F** Representative images from one mouse of ipsilateral and contralateral projections from the BLA to the ventral striatum following injection as in **E**. These example images show that while some BLA neurons transverse into the contralateral ventral striatum, qualitatively, the bulk of input is ipsilateral. **G** Diagram of approach for identifying BLA *Drd1*⁺ and *Drd2*⁺ projecting neurons to the NAc and TuS in the ventral striatum. **H** Percentage of the *Drd1*⁺ and *Drd2*⁺ neurons within the BA that project to the NAc (red), TuS (green), or both (yellow) ($n = 3$ mice/genotype, 2/1/sex, 5–6 sections/mouse). **I** Representative image of a retrograde injection in a *Drd1*-Cre mouse and **J** the anterior to posterior span of VS projecting BLA neurons. Scale bars = 500 μ m. PCx piriform cortex, NAcC and NAcSh nucleus accumbens core and shell, respectively, BLA basolateral amygdala, BA basal amygdala, LA lateral amygdala.

project to the NAc, and ~21% project to both (Fig. 2H–J). We found a more even split between the *A2a*⁺ ventral striatum projecting BLA neurons, with ~44% projecting to the TuS, 42% projecting to the NAc, and ~14% projecting to both. Thus, a subset of BLA projection neurons innervate both ventral striatum targets (Fig. 2H, right). Taken together, these tracing results establish that both *Drd1*⁺ and *Drd2*⁺ neurons, largely from the BA, innervate the ventral striatum.

***Drd1*⁺ and *Drd2*⁺ BLA neurons excite ventral striatum spiny projection neurons**

Next, we injected a Cre-dependent AAV expressing channelrhodopsin and EYFP (AAV.Ef1a.DIO.hChR2(E123T/T159C)-EYFP) or EYFP alone as a control (AAV.Ef1a.DIO.EYFP) into the BLA of *Drd1*-Cre and *A2a*-Cre mice, which were crossed with the Ai9 tdTomato Cre reporter line. Later we took coronal slices of the ventral striatum for ex vivo recordings to determine which ventral striatum spiny projection neurons (SPNs) the BLA neurons make synapses upon. tdTomato⁺ neurons were identified and used to identify *Drd1*⁺ or *Drd2*⁺ SPNs (those expressing tdTomato⁺ in either *Drd1*-Cre or *A2a*-Cre mice respectively; Fig. 3Ai & Aii). In the same slices we also patched onto tdTomato⁺ SPNs to monitor activity of *Drd1* \emptyset and *Drd2* \emptyset (putative *Drd2*⁺ or *Drd1*⁺) SPNs, in either *Drd1*-Cre or *A2a*-Cre mice respectively. During recordings, blue light pulses were delivered to excite ChR2-expressing BLA terminals in the ventral striatum. As stated above, there is minimal co-expression of *Drd1* and *Drd2* in the same cells in both the BLA and ventral striatum (Supplementary Fig. 2A & B). Moreover, the BLA to ventral striatum projection is predominantly ipsilateral (Fig. 2E, F). Current injection into ventral striatum neurons confirmed their firing patterns are as expected for TuS SPNs (Supplementary Fig. 3A & B) [45].

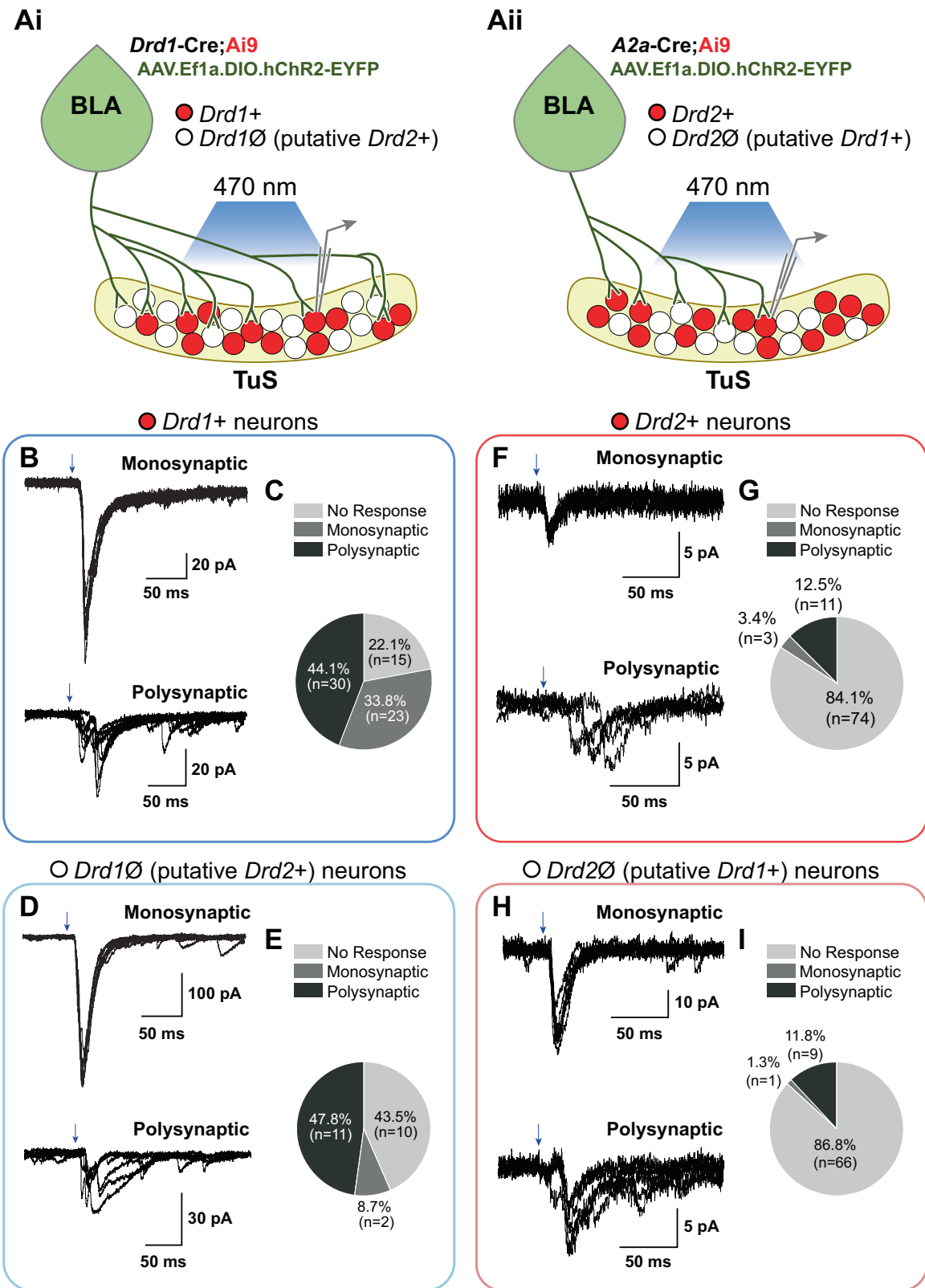
We found that both BLA cell populations synapse upon both *Drd1*⁺ and *Drd2*⁺ SPNs, albeit with differing proportions and strengths of responses. The majority of *Drd1*⁺ BLA neurons elicited large monosynaptic currents in *Drd1*⁺ (mean = 74.46 pAmp, SEM = 7.55 pAmp, $n = 23$) and *Drd1* \emptyset SPNs (mean = 186.1 pAmp, SEM = 100.2, $n = 3$, Fig. 3B–E). While both ventral striatum cell types were excited by *Drd1*⁺ BLA neurons, BLA *Drd1*⁺ neurons send stronger input (viz., larger evoked excitatory postsynaptic currents [EPSCs]) and do so more predominantly upon *Drd1*⁺ vs *Drd1* \emptyset (putative *Drd2*⁺) SPNs (*Drd1*⁺ vs *Drd1* \emptyset monosynaptic: $\chi^2(1, N = 91) = 5.45$, $p = 0.02$; *Drd1*⁺ vs *Drd1* \emptyset polysynaptic: $\chi^2(1, N = 91) = 0.096$, $p = .757$; Fig. 3C & E). In a subset of SPNs, monosynaptic glutamatergic connections were verified via pharmacological manipulations (Supplementary Fig. 3C & D). Likewise, *Drd2*⁺ BLA neurons also synapse upon *Drd2*⁺ and *Drd2* \emptyset SPNs, but compared to the *Drd1*⁺ BLA input, input from *Drd2*⁺ BLA neurons was both weaker (mean monosynaptic current in *Drd2*⁺ SPN = 10.79 pAmp, SEM = 2.78 pAmp, $n = 3$; mean monosynaptic current in *Drd2* \emptyset SPN = 36.74 pAmp, SEM = 1.98 pAmp, $n = 1$) and not as predominant (Fig. 3F–I). A far larger percentage of SPNs displayed monosynaptic EPSCs upon *Drd1*⁺ BLA neuron terminal stimulation

than when stimulating *Drd2*⁺ BLA terminals ($\chi^2(1, N = 255) = 33.947$, $p < 0.001$). Including polysynaptic EPSCs, 13.1–15.9% of SPNs (*Drd2*⁺ and *Drd2* \emptyset , respectively) displayed evoked potentials, and these were notably modest in amplitude compared to what was observed when stimulating *Drd1*⁺ BLA terminals (e.g., Fig. 3B vs F). Together these results extend the anatomical circuitry (Fig. 1 & 2) by showing that both *Drd1*⁺ and *Drd2*⁺ BLA neurons excite ventral striatum spiny projection neurons.

Both *Drd1*⁺ BLA neurons innervating the NAc and *Drd2*⁺ BLA neurons innervating the TuS promote avoidance behavior

Next, we sought to determine a functional role for BLA *Drd1*⁺ and *Drd2*⁺ input to the ventral striatum. In the first assay, we used an optogenetic approach to excite *Drd1*⁺ and *Drd2*⁺ BLA neuron terminals innervating either the NAc or TuS to determine if these pathways influence avoidance or approach behaviors. For this we unilaterally injected *Drd1*-Cre and *A2a*-Cre mice with AAV.Ef1a.DIO.hChR2(E123T/T159C)-EYFP or AAV.Ef1a.DIO.EYFP as control into their BLA and later implanted optical fibers into the ipsilateral NAc or TuS (Fig. 4A). Given the similar BLA innervation of both the NAc core and shell (Fig. 2C), we targeted both NAc subregions for stimulation (Supplementary Fig. 4A, B). Four weeks post injection, we used a 3-chamber real-time place preference/aversion assay wherein light was delivered to stimulate the *Drd1*⁺ or *Drd2*⁺ BLA neuron terminals (465 nm, 15 ms pulses, 40 Hz) on only one side of the chamber, with no optical stimulus in either the center or the opposite chambers (Fig. 4B). The location of the mice was tracked with infrared photobeams to trigger optogenetic stimulation, and video was captured for off-line quantification.

We found that optical stimulation of *Drd1*⁺ BLA→NAc neuron terminals resulted in less time spent in the light-paired chamber compared to optical stimulation of *Drd2*⁺ BLA→NAc neuron terminals and EYFP controls (Fig. 4Ci & Cii) (One-way ANOVA $F(2,18) = 5.04$, $p = 0.018$). The EYFP control groups were collapsed across genotypes, containing both *Drd1*-Cre and *A2a*-Cre mice with the same optic fiber placement, since these behavioral results were not different from each other (percent of time spent in non-paired side for *Drd1*⁺ vs *A2a* + NAc EYFP controls unpaired t -test, $t(6) = 1.85$, $p = 0.1134$; and *Drd1*⁺ vs *A2a* + TuS EYFP controls unpaired t -test, $t(6) = 0.305$, $p = 0.771$). Indeed, compared to the non-stimulated side, mice spent $49.70 \pm 11.10\%$ (mean \pm SEM) less time on the chamber paired with *Drd1*⁺ BLA→NAc neuron terminal stimulation ($t(6) = 2.981$, $p = 0.025$). Similarly, we found that optical stimulation of *Drd2*⁺ BLA→TuS neuron terminals resulted in less time spent in the light-paired chamber compared to optical stimulation of EYFP + BLA→TuS controls (Fig. 4Di & Dii) (Welch's ANOVA $W(2.00,8.31) = 6.02$, $p = 0.024$). Compared to the non-stimulated side, mice spent $31.42 \pm 6.39\%$ (mean \pm SEM) less time on the chamber paired with *Drd2*⁺ BLA→TuS neuron terminal stimulation ($t(5) = 2.916$, $p = 0.033$). These results show that activation of *Drd1*⁺ and *Drd2*⁺ BLA input to the NAc and TuS respectively lead to avoidance behavior.



***Drd1*+ BLA neurons innervating the NAc and *Drd2*+ BLA neurons innervating the TuS support pavlovian fear learning**

Next, we wanted to know the possible influence of these pathways on learned emotional behaviors. To do this we employed an odor-shock Pavlovian fear-learning paradigm [36,

46, 47] wherein an otherwise neutral odor is paired with a mild foot shock (Supplementary Fig. 5Ai). To quantify learning, we monitored both physical immobility and fear-associated respiratory power (4–6 Hz) which increases in power when animals anticipate an aversively-paired stimulus [36, 48]. Mice were placed

Fig. 3 Synaptic properties of *Drd1* and *Drd2* expressing ventral striatum neurons receiving BLA neuronal projections. **Ai** Schematic indicating Cre-dependent expression of ChR2 in *Drd1*+ BLA neurons of *Drd1*-Cre;Ai9 mice. In these mice, tdTomato+ neurons are presumably *Drd1*+ and tdTomato- neurons are presumably *Drd1*0. During whole-cell patch clamp recordings, ChR2 expressing BLA terminals were activated by 470 nm light. **Aii** Schematic indicating Cre-dependent expression of ChR2 in *Drd2*+ BLA neurons of *A2a*-Cre;Ai9 mice. tdTomato+ neurons are presumably *Drd2*+, and tdTomato- neurons are presumably *Drd2*0. **B** Example light-evoked monosynaptic EPSCs (top) and light-evoked polysynaptic EPSCs (bottom) from *Drd1*+ TuS neurons under voltage clamp mode. **C** Neurons organized by response type upon stimulation of *Drd1*+ TuS projecting BLA terminals. **D** Example evoked EPSCs from *Drd1*0 TuS neurons. **E** Neurons organized by response type upon stimulation of *Drd1*0 TuS projecting BLA terminals. **F** Example evoked EPSCs from *Drd2*+ TuS neurons. **G** Neurons organized by response type upon stimulation of *Drd2*+ TuS projecting BLA terminals. **H** Example evoked EPSCs from *Drd2*0 TuS neurons. **I** Neurons organized by response type upon stimulation of *Drd2*+ TuS projecting BLA terminals. The holding potential was -70 mV. *Drd1*-Cre;Ai9 $n = 2M/1F$, *A2a*-Cre;Ai9 $n = 4F/4M$.

in a plethysmograph with a custom floor made out of metal connected to a shock stimulus generator. Also connected to the plethysmograph was a tube allowing delivery of clean air or an odor which were both controlled by an odor presentation machine. All behavioral measures and stimuli were controlled by the same computer allowing synchrony in measures and stimulus presentation events. In untreated C57BL/6J mice, we validated that only odors paired with shock were associated with elevations in physical immobility following the conditioning day (Supplementary Fig. 5B). We also validated that fear-associated 4–6 Hz respiratory power is similarly elevated as mice learn to associate an odor with a shock (Supplementary Fig. 5C–H).

We used a chemogenetic approach to suppress BLA→ventral striatum input which included six separate groups of mice to establish the roles of each of the BLA→NAc and BLA→TuS pathways (Fig. 5A). These included *Drd1*+ and *Drd2*+ mice injected with rgAAV.hSyn.DIO.hM4D(Gi)-mCherry or rgAAV.hSyn.DIO-mCherry as control. All mice were subsequently implanted with bilateral intracranial cannulae into the BLA for administration of either the DREADD ligand J60 [35] or vehicle (Supplementary Fig. 6A, B). J60 or vehicle were administered 30 min prior to the learning session following a single behavioral session on a prior day to acclimate the mice to the chamber.

Among both the BLA→NAc and BLA→TuS groups, all control groups displayed elevations in fear-associated respiration by the 10th trial of odor-shock pairings (Fig. 5B, C & F, G; NAc mCherry control: Two-way RM ANOVA, trial main effect $F(1,27) = 86.2$, $p < 0.001$; TuS mCherry control: Two-way RM ANOVA, trial main effect $F(1,29) = 151$, $p < 0.001$) indicating that they learned to associate an odor with an aversive outcome. Like in the opto-RTPP/A behavioral assay, these control groups were collapsed across genotypes so they contained both *Drd1*-Cre and *Drd2*-Cre mice since these behavioral results were not different from each other (All Two-way RM ANOVAs genotype main effect: vehicle treated *Drd1*-Cre vs *Drd2*-Cre NAc mCherry controls, $F(1,13) = 0.359$, $p = 0.559$; J60 treated *Drd1*-Cre vs *Drd2*-Cre NAc mCherry controls, $F(1,12) = 0.323$, $p = 0.580$; vehicle treated *Drd1*-Cre vs *Drd2*-Cre TuS mCherry controls, $F(1,14) = 0.181$, $p = 0.677$; and J60 treated *Drd1*-Cre vs *Drd2*-Cre TuS mCherry controls, $F(1,13) = 3.58$, $p = 0.081$). As expected, similar elevations in physical immobility were also observed (Supplementary Fig. 7). Importantly, there was no difference in learning between the vehicle and J60 infused groups supporting that there are no off-target effects of this DREADD ligand on odor-shock learning (Fig. 5B, C & F, G; NAc mCherry controls Trial 10: MLSD = |Vehicle-J60| = -0.0443 , $p = 0.601$, TuS mCherry controls Trial 10: MLSD = |Vehicle-J60| = 0.0118 , $p = 0.888$).

While neither inhibition of *Drd2*+ BLA→NAc nor *Drd1*+ BLA→TuS pathways impacted fear-learning (Fig. 5E & H, Two-way RM ANOVA, trial main effect: *Drd2*+ BLA→NAc: $F(1,13) = 301$, $p < 0.001$; *Drd1*+ BLA→TuS: $F(1,13) = 85.6$, $p < 0.001$), we found that inhibition of *Drd1*+ BLA→NAc and *Drd2*+ BLA→TuS pathways suppressed the magnitude of the learned association. Both *Drd1*+ BLA→NAc and *Drd2*+ BLA→TuS pathway inhibition resulted in less fear-related respiration by trial 10 in J60 infused mice compared to those infused with

vehicle (Fig. 5D & I; *Drd1*+ BLA→NAc Trial 10: MLSD = |Vehicle-J60| = 0.319 , $p = 0.049$, *Drd2*+ BLA→TuS Trial 10: MLSD = |Vehicle-J60| = 0.364 , $p < 0.001$). Fear-related physical immobility was likewise reduced upon *Drd2*+ BLA→TuS pathway inhibition, yet interestingly not upon *Drd1*+ BLA→NAc inhibition (Supplementary Fig. 7). These results show that *Drd1*+ and *Drd2*+ BLA input to the NAc and TuS respectively are necessary for fear learning in addition to their role in real-time avoidance.

DISCUSSION

It is well established that BLA outputs to specific brain regions influence emotional responses (e.g., [15, 49–54]). More recently, several lines of evidence have uncovered divergent valence responding through genetically-distinct neurons within the BLA, including by means of *Ppp1r1b* and *Rspo2* neurons [17–19]. Together, both the genetic identity and downstream targets of BLA neurons are necessary to incorporate when understanding the role of BLA cell types in orchestrating the many functions of the BLA.

In the present study we focused on defining the contributions of *Drd1*+ and *Drd2*+ BLA neurons to emotional responding. The *Drd1* and *Drd2* genes encode for the D1 and D2 receptors, respectively [24], which regulate PPP1R1B – a marker for one of the two main classes of BLA excitatory neurons. It has been long known that D1 and D2 receptors are in the BLA (e.g., [55]). We established that both *Drd1*+ and *Drd2*+ BLA neurons innervate the NAc and TuS, and we subsequently focused upon these two pathways (BLA→NAc and BLA→TuS) given the recent evidence of regulation of emotional responses through BLA output into these regions [17]. Our findings extend the work of [17] by showing that in addition to the *Rspo2/Fezf2* BLA neuron class, both *Drd1*+ and *Drd2*+ BLA neurons in the *Ppp1r1b* neuron class also each innervate the NAc and TuS. These neurons originate from nearly the entire anterior-posterior extent of the BLA, and specifically the vast majority from within the BA (Fig. 1). A small population of *Drd1*+ and *Drd2*+ BLA neurons even send collaterals to both the NAc and TuS. Further, our synaptophysin tracing suggests that these BLA neuron populations innervate nearly all TuS and NAc subregions (all layers of TuS and both the NAc core and shell; Fig. 2). While the spatial innervation of *Drd1*+ and *Drd2*+ BLA neurons into the ventral striatum is not unlike that reported by [17], it is important to emphasize that *Fezf2*+ BLA neurons do not co-express PPP1R1B [17], which suggests these three neuron types connecting the BLA with the ventral striatum are distinct.

While the synaptophysin tracing suggests synaptic innervation of the ventral striatum by *Drd1*+ and *Drd2*+ BLA neurons, we used brain slice recordings to quantify this. This is interesting given that the primary cell type in the ventral striatum are spiny projection neurons which also express *Drd1*+ and *Drd2*+. We focused our recordings on TuS spiny projection neurons given the comparable innervation of both structures (NAc and TuS) by *Drd1*+ and *Drd2*+ BLA neurons which allowed us to also perform recordings to identify if there is logic by which ventral striatum neurons these

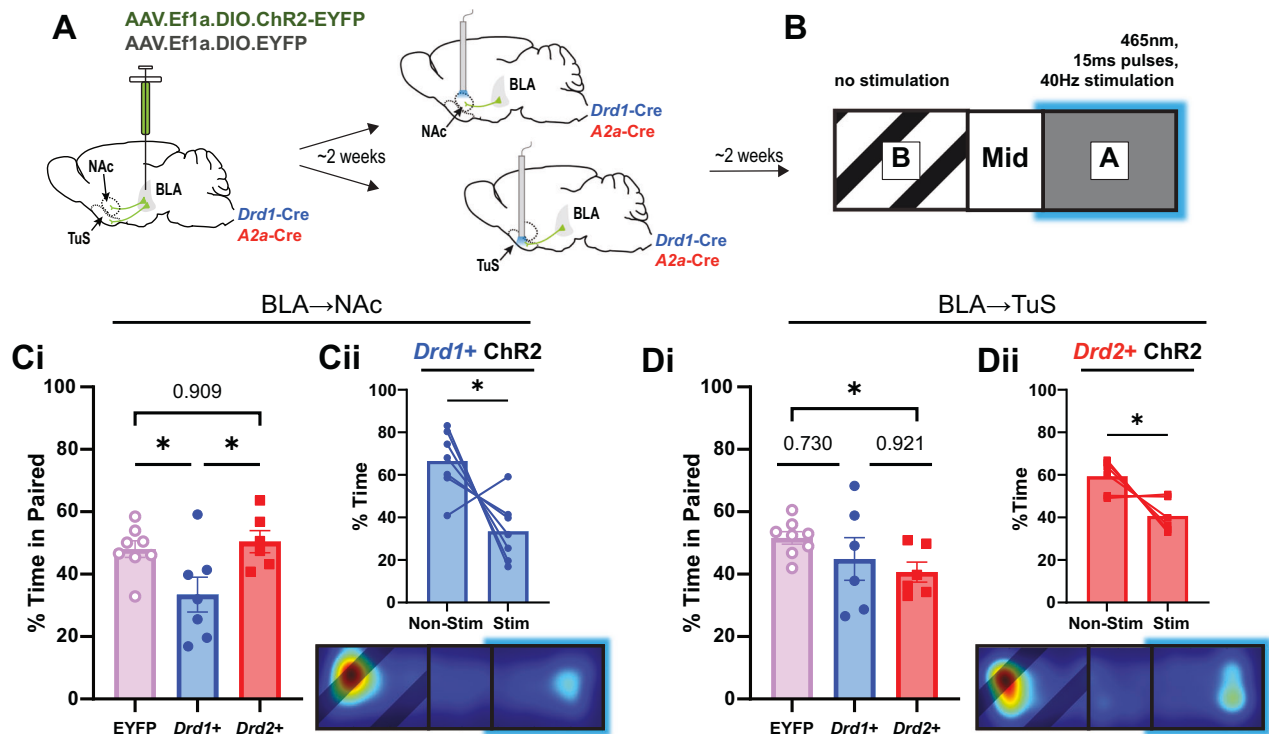


Fig. 4 BLA *Drd1*⁺ and *Drd2*⁺ neurons innervating the ventral striatum promote aversive states depending upon projection target.

A Paradigm for optic activation of NAc or TuS projecting *Drd1*⁺ or *Drd2*⁺ BA neurons and **B** 3-chamber real-time place preference/aversion assay where optic stimulation occurs in only one side of the chamber (chamber A, blue glow). **Ci** Optical stimulation of *Drd1*⁺ BLA→NAc neurons resulted in less time spent in the light-paired chamber ($*p < 0.05$, One-way ANOVA, $F(2,18) = 5.04$, $p = 0.018$, EYFP controls $n = 4M/4F$, *Drd1*⁺ ChR2 $n = 3M/4F$, *Drd2*⁺ ChR2 $n = 3M/3F$). **Cii** Stimulation of *Drd1*⁺ BLA→NAc neurons results in avoidance of the light-paired chamber (upper, $t(6) = 2.981$, $*p = 0.025$), demonstrated by representative heat map of chamber preference from one mouse (lower). **Di** Optical stimulation of *Drd2*⁺ BLA→TuS neurons resulted in less time spent in the light-paired chamber compared to optical stimulation of EYFP controls ($*p < 0.05$, Welch's ANOVA $W(2.00,8.31) = 6.02$, $p = 0.024$, EYFP controls $n = 6M/2F$, *Drd1*⁺ ChR2 $n = 2M/4F$, *Drd2*⁺ ChR2 $n = 2M/4F$). **Dii** Stimulation of *Drd2*⁺ BLA→TuS neurons results in avoidance of the light-paired chamber (upper, $t(5) = 2.916$, $*p = 0.033$), demonstrated by representative heat map of chamber preference from one mouse (lower). EYFP control groups were collapsed across genotypes, containing both *Drd1*-Cre and *A2a*-Cre mice, since these behavioral results were not different from each other (percent of time spent in non-paired side for *Drd1*⁺ vs *Drd2*⁺ NAc EYFP controls unpaired t -test, $t(6) = 1.85$, $p = 0.1134$; and *Drd1*⁺ vs *Drd2*⁺ TuS EYFP controls unpaired t -test, $t(6) = 0.305$, $p = 0.771$). Behaviors did not differ by sex (all unpaired t -tests: NAc YFP $t(6) = 1.29$, $p = 0.245$; NAc *drd1*⁺ ChR2 $t(5) = 0.933$, $p = 0.394$; NAc *drd2*⁺ ChR2 $t(4) = 0.309$, $p = 0.772$; TuS YFP $t(6) = 1.10$, $p = 0.315$; TuS *Drd1*⁺ ChR2 $t(4) = 0.818$, $p = 0.459$; TuS *Drd2*⁺ ChR2 $t(4) = 0.253$, $p = 0.813$; Mean \pm SEM).

BLA neurons synapse upon. We found that both BLA cell types excite *Drd1*⁺ and *Drd2*⁺ (identified in this experiment by expression of *A2A*) TuS neurons in manners which appeared to be predominately glutamatergic, with especially *Drd1*⁺ BLA neurons sending a large amount of monosynaptic currents (Supplementary Fig. 3). Further, *Drd1*⁺ BLA neurons monosynaptically excited predominately *Drd1*⁺ TuS neurons, and *Drd2*⁺ BLA neurons non-preferentially excited a small population of both *Drd1*⁺ and *Drd2*⁺ TuS neurons. While these results were initially surprising given that the *Drd1*⁺ BLA→TuS pathway was dispensable for the fear and avoidance behaviors explored in this work, this may indicate a potential role for this pathway in other behaviors, such as those involved in reward. Thus, BLA input to the TuS, and therefore possibly also the NAc, has an organization which allows for recruitment of specific postsynaptic neurons in the TuS which could therefore allow differential output from the ventral striatum in manners supporting specific outputs into the basal ganglia and other brain networks important for behavioral responses.

We found within this circuitry that the parallel pathways generated by the *Drd1*⁺ and *Drd2*⁺ BLA neuron populations modulate negative emotional states depending upon their ventral striatum projection target (Fig. 6). To show this, we used two distinct behavioral paradigms in combination with either

projection specific chemo- or optogenetic manipulations. In all behavioral paradigms, we were able to uncover a role for either *Drd1*⁺ and/or *Drd2*⁺ neurons, yet, in not all cases did each cell population impact behavior. Instead, the impact on behavior was in most cases also projection target specific. For instance, *Drd1*⁺ BLA neurons innervating the NAc increased negative valence states in the real-time place preference/aversion paradigm, whereas the same cell population projecting to the TuS did not (Fig. 4). Likewise, *Drd2*⁺ BLA neurons innervating the TuS increased negative valence states in the real-time place preference/aversion paradigm, whereas the same cell population projecting to the NAc did not. Similar differences in how these genetically-distinct BLA cell populations influenced Pavlovian fear learning were also observed to be cell-type and projection target specific. These findings lay the foundation for future work to systematically target *Drd1*⁺ or *Drd2*⁺ BLA inputs into specific regions within the NAc (core vs shell [56]) or TuS (medial vs lateral [57, 58]) which may provide even more specific behavioral outcomes. This work extends a role for *Drd1*⁺ BLA neuron output to the central amygdala, which was found to influence extinction memory [26], into two ventral striatum subregions which are important for valence-based behavioral responses, and allows for comparison with the influence of the neighboring *Drd2*⁺ neurons.

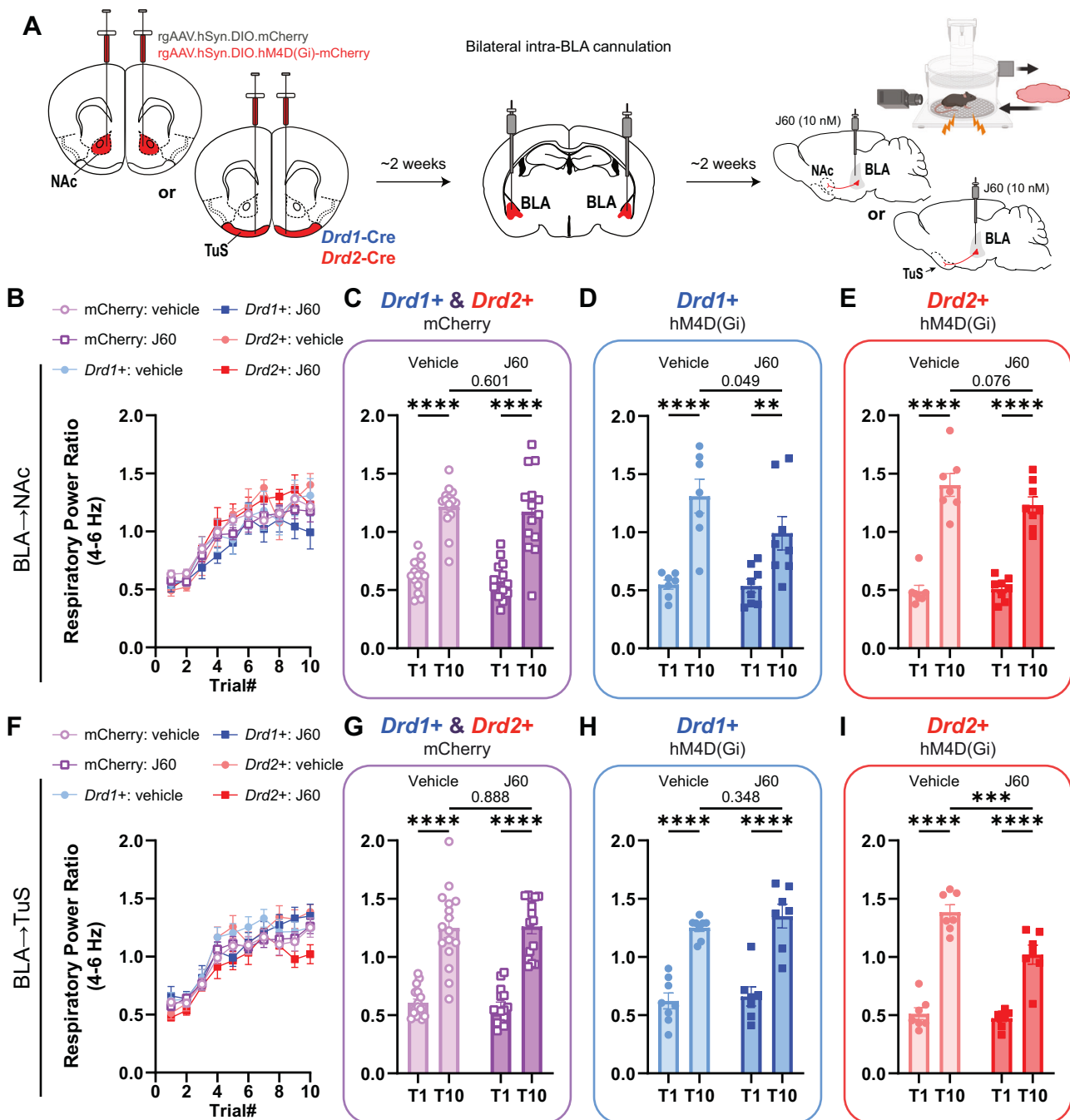


Fig. 5 BLA *Drd1+* and *Drd2+* neurons innervating the ventral striatum support pavlovian fear learning depending upon projection target. **A** Paradigm for DREADD induced silencing of NAc or TuS projecting *Drd1+* or *Drd2+* BLA cells. Some aspects created in <https://BioRender.com>. **B** Influence of DREADD agonist J60 (100 nL, 10 nM) on fear learning in all NAc injected mice, **C** left NAc injected mCherry controls (**** $p < 0.0001$, Two-way RM ANOVA, Trial main effect $F(1,27) = 86.2$, $p < 0.001$, $n = 10M/19F$); **D** middle *Drd1+* hM4D(Gi) mice (**** $p < 0.0001$, ** $p < 0.01$, Two-way RM ANOVA, Trial main effect $F(1,13) = 48.9$, $p < 0.001$, $n = 6M/9F$); and **E** right *Drd2+* hM4D(Gi) mice (**** $p < 0.0001$, Two-way RM ANOVA, Trial main effect $F(1,13) = 301$, $p < 0.001$, $n = 8M/7F$). **F** Influence of DREADD agonist J60 (100 nL, 10 nM) on fear learning in all TuS injected mice, **G** left mCherry TuS injected controls (**** $p < 0.0001$, Two-way RM ANOVA, Trial main effect $F(1,29) = 151$, $p < 0.001$, $n = 15M/16F$); **H** middle *Drd1+* hM4D(Gi) mice (**** $p < 0.0001$, Two-way RM ANOVA, Trial main effect $F(1,13) = 85.6$, $p < 0.001$, $n = 7M/8F$); and **I** right *Drd2+* hM4D(Gi) mice (**** $p < 0.001$, **** $p < 0.0001$, Two-way RM ANOVA, $F(1,12) = 7.71$, $p = 0.017$, $n = 7M/8F$). mCherry control groups were collapsed across genotypes, containing both *Drd1*-Cre and *Drd2*-Cre mice since these behavioral results were not different from each other (All Two-way RM ANOVAs genotype main effect: vehicle treated *Drd1*-Cre vs *Drd2*-Cre NAc mCherry controls, $F(1,13) = 0.359$, $p = 0.559$; J60 treated *Drd1*-Cre vs *Drd2*-Cre NAc mCherry controls, $F(1,12) = 0.323$, $p = 0.580$; vehicle treated *Drd1*-Cre vs *Drd2*-Cre TuS mCherry controls, $F(1,14) = 0.181$, $p = 0.677$; and J60 treated *Drd1*-Cre vs *Drd2*-Cre TuS mCherry controls, $F(1,13) = 3.58$, $p = 0.081$). Behaviors differed by sex for *Drd1+* hM4D(Gi) mice suggesting sex differences in output to NAc among *Drd1+* neurons (all Three-way ANOVAs for sex main effect: NAc mCherry controls $F(1,25) = 0.0354$, $p = 0.852$; *Drd1+* hM4D(Gi) NAc $F(1,11) = 14.0$, $p = 0.003$; *Drd2+* hM4D(Gi) NAc $F(1,11) = 0.215$, $p = 0.652$; TuS mCherry controls $F(1,27) = 2.81$, $p = 0.102$; *Drd1+* hM4D(Gi) TuS $F(1,11) = 0.617$, $p = 0.449$; *Drd2+* hM4D(Gi) TuS $F(1,10) = 0.474$, $p = 0.507$. Mean \pm SEM.

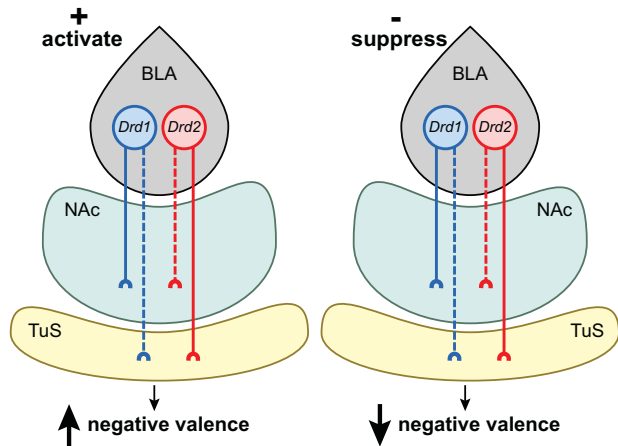


Fig. 6 Overview of findings illustrating the behavioral consequences of activating (left) or suppressing (right) *Drd1*+ or *Drd2*+ BLA neuron inputs to the NAc and TuS. Solid lines annotate pathways found herein to play a role in real-time avoidance and learned aversion. Dashed lines indicate pathways that were not found to support either of those behaviors/states, at least using the approaches applied in the present study.

Interestingly, when comparing changes in fear-associated respiration (well known to be influenced by sympathetic state [36, 48, 59–61]) and fear-induced immobility, we saw that manipulation of NAc projecting *Drd1*+ BLA neurons did not similarly influence both of those fear-associated behaviors (Supplementary Fig. 7). This may be due to either distinct inputs or outputs (collaterals) of the *Drd1*+ BLA neurons which might differentially guide changes in respiratory behavior versus motor behavior. For instance, differential innervation of the periaqueductal grey might allow for one cell-type to influence respiration over another given the periaqueductal grey's influence on breathing [62, 63]. While we did not identify the differential pathway, it is interesting to find such instances wherein fear-related behaviors are not simultaneously displayed. Further manipulation of this pathway while similarly taking multiple measures of fear-related behaviors, including even heart rate, skin conductance, and ultrasonic vocalizations for instance, will help refine our understanding of circuitry which specifically supports each to be displayed during emotional contexts.

Given the fact that these BLA→ventral striatum neurons express dopamine receptors, it is tempting to speculate how this pathway may be modulated by dopamine. Dopamine within the BLA is necessary for fear learning [25]. Local antagonism of both D1Rs and D2Rs within the BLA blocks the expression of fear during a potentiated startle paradigm [64, 65]. Antagonism of BLA D1Rs also perturbs the timing of fear behavior [66], and antagonism of BLA D2Rs attenuates freezing during Pavlovian fear conditioning [27, 28, 67]. The role of dopamine receptors is similarly mixed in appetitive behaviors, where antagonizing both D1Rs and D2Rs within the BLA attenuates conditioned reward seeking and taking [29, 68, 69]. Indeed, local application of D1 agonists increases intrinsic excitability and the evoked firing of BLA neurons [70]. D1 receptors have a lower affinity for dopamine than D2 receptors [71, 72]. Further, when dopamine levels are low, D2 receptors are agonized, but when DA levels are elevated, like when receiving an emotionally salient stimulus, both D1 and D2 receptors become agonized [73–75]. It is possible these differential roles of D1 and D2 receptors in the BLA might explain our finding that *Drd2*+ neurons vs *Drd1*+ neurons contributed differently to the regulation of emotional states.

Several findings throughout this study pose the need to caveat some interpretations. First, while the fiber optic implants in the NAc extended ~1 mm over the TuS, and blue light used in our approach would not penetrate more than ~800 µm through brain,

we cannot rule-out that no BLA terminals in the TuS were activated upon NAc stimulation. Related to that, the finding that a subpopulation of *Drd1*+ and *Drd2*+ BLA neurons send collaterals to both the NAc and TuS means that the parallel circuitry generated by these genetically-distinct pathways is considerably complicated. This also adds a caveat to the optical stimulation results indicating *Drd1*+ BLA→NAc neurons influence avoidance since Chr2-mediated activation of those terminals in the NAc might have activated TuS-projecting BLA neurons through antidromic stimulation. Further, while we know that some BLA neurons cross the midline (e.g., Fig. 2F), we did not attempt to disambiguate the role of ipsi- vs contralateral *Drd1*+ and *Drd2*+ BLA pathways. Although it is notable that during preparation of this paper, a report was published [76] implicating BLA projections to the NAc in valence behaviors which appear to differ depending upon if they transverse through the anterior commissure. Additionally, in experiments wherein AAV injections were performed in the BLA, in some cases, small populations of neurons were labeled outside of the BLA which may impact results. That stated, among amygdaloid nuclei, multiple separate experiments support that it is principally neurons in the BLA which innervate the TuS and NAc (Fig. 1 & Supplementary Fig. 1). Finally, while both our results and that from prior work support that there are more *Drd1*+ neurons in the BLA than *Drd2*+ (Fig. 1 and [40]), which was also evident when analyzing levels of *A2a*+ neurons in the BLA, we found that recombination occurred only in a subpopulation of Cre-expressing neurons (Supplementary Fig. 8). This was especially the case in the *Drd2*-Cre line. The fact that our chemo- and opto-genetic experiments resulted in behavioral changes (Fig. 4 & 5, Supplementary Fig. 7), despite our approaches not capturing the entire population of Cre-expressing neurons, reflects that these pathways are potent modulators of emotions. Indeed, even chemogenetic manipulation *Drd2*+ BLA neurons, of which only a sparse population showed recombination efficiency, impacted emotional outcomes (Supplementary Fig. 7). These stated, the low recombination efficiency among *Drd2*+ BLA neurons supports the need for future research to thoroughly understand the role of *Drd2*+ BLA projections to the NAc since we cannot confidently exclude this pathway from being involved in fear-learning, nor other learned aversive states.

Overall, this work has uncovered that *Drd1*+ and *Drd2*+ neurons within the *Ppp1r1b* BLA neuron class form parallel pathways which influence emotional states when they are activated or suppressed and do so depending upon where they synapse – with unique contributions of *Drd1*+ and *Drd2*+ BLA→NAc vs BLA→TuS circuitry on negative valence states. Given the connectivity to the TuS especially, given its established roles in sensory processing [20], it is interesting to consider if these pathways may contribute to changes in sensory processing in individuals who suffer from anxiety disorders [77]. Overall, our results contribute to a model whereby parallel, genetically-distinct BLA to ventral striatum circuits inform emotional states in a projection-specific manner. This work adds to our understanding of the complex interplay between projection cell types and their projection targets, in how the BLA helps orchestrate emotions.

CODE AVAILABILITY

MATLAB code used to extract respiratory frequency can be available upon request to the corresponding author.

REFERENCES

1. Klüver H, Bucy PC. Preliminary analysis of functions of the temporal lobes in monkeys. *Arch Neurol Psychiatry*. 1939;42:979–1000.
2. Blanchard DC, Blanchard RJ. Innate and conditioned reactions to threat in rats with amygdaloid lesions. *J Comp Physiol Psychol*. 1972;81:281–90.

3. Zald DH, Pardo JV. Emotion, olfaction, and the human amygdala: amygdala activation during aversive olfactory stimulation. *Proc Natl Acad Sci USA*. 1997;94:4119–24. <http://www.pnas.org/content/94/8/4119.abstract>.
4. Weiskrantz L. Behavioral changes associated with ablation of the amygdaloid complex in monkeys. *J Comp Physiol Psychol*. 1956;49:381–91. <https://psycnet.apa.org/journals/com/49/4/381>.
5. Cahill L, McGaugh JL. Amygdaloid complex lesions differentially affect retention of tasks using appetitive and aversive reinforcement. *Behav Neurosci*. 1990;104:532–43.
6. LeDoux JE. Brain mechanisms of emotion and emotional learning. *Curr Opin Neurobiol*. 1992;2:191–7. http://www.ncbi.nlm.nih.gov/entrez/query.fcgi?cmd=Retrieve&db=PubMed&dopt=Citation&list_uids=1638153.
7. Maren S, Aharonov G, Fanselow MS. Retrograde abolition of conditional fear after excitotoxic lesions in the basolateral amygdala of rats: absence of a temporal gradient. *Behav Neurosci*. 1996;110:718–26.
8. Cousens G, Otto T. Both pre- and posttraining excitotoxic lesions of the basolateral amygdala abolish the expression of olfactory and contextual fear conditioning. *Behav Neurosci*. 1998;112:1092–103.
9. Hatfield T, Han J-S, Conley M, Gallagher M, Holland P. Neurotoxic lesions of basolateral, but not central, amygdala interfere with pavlovian second-order conditioning and reinforcer devaluation effects. *J Neurosci*. 1996;16:5256–65. <http://www.jneurosci.org/content/16/16/5256.abstract>.
10. Setlow B, Gallagher M, Holland PC. The basolateral complex of the amygdala is necessary for acquisition but not expression of CS motivational value in appetitive pavlovian second-order conditioning. *Eur J Neurosci*. 2002;15:1841–53. <https://doi.org/10.1046/j.1460-9568.2002.02010.x>.
11. Schoenbaum G, Setlow B, Nugent SL, Saddoris MP, Gallagher M. Lesions of orbitofrontal cortex and basolateral amygdala complex disrupt acquisition of odor-guided discriminations and reversals. *Learn Mem*. 2003;10:129–40.
12. Maren S, Quirk GJ. Neuronal signalling of fear memory. *Nat Rev Neurosci*. 2004;5:844–52.
13. Rogan MT, Staubli UV, LeDoux JE. Fear conditioning induces associative long-term potentiation in the amygdala. *Nature*. 1997;390:604–7. http://www.ncbi.nlm.nih.gov/entrez/query.fcgi?cmd=Retrieve&db=PubMed&dopt=Citation&list_uids=9403688.
14. LeDoux J. The emotional brain, fear, and the amygdala. *Cell Mol Neurobiol*. 2003;23:727–38. http://www.ncbi.nlm.nih.gov/entrez/query.fcgi?cmd=Retrieve&db=PubMed&dopt=Citation&list_uids=14514027.
15. Namburi P, Beyeler A, Yorozu S, Calhoun G, Halbert S, Wichmann R, et al. A circuit mechanism for differentiating positive and negative associations. *Nature*. 2015;520:675–8. <https://pubmed.ncbi.nlm.nih.gov/25925480/>.
16. Hochgerner H, Singh S, Tibi M, Lin Z, Skarbiak N, Admati I, et al. Neuronal types in the mouse amygdala and their transcriptional response to fear conditioning. *Nat Neurosci*. 2023;26:2237–49. <https://doi.org/10.1038/s41593-023-01469-3>.
17. Zhang X, Guan W, Yang T, Furlan A, Xiao X, Yu K, et al. Genetically identified amygdala–striatal circuits for valence-specific behaviors. *Nat Neurosci*. 2021;24:1586–600. <https://doi.org/10.1038/s41593-021-00927-0>.
18. Kim J, Zhang X, Muralidhar S, LeBlanc SA, Tonegawa S. Basolateral to central amygdala neural circuits for appetitive behaviors. *Neuron*. 2017;93:1464–79.e5. <http://www.sciencedirect.com/science/article/pii/S0896627317301423>.
19. Kim J, Pignatelli M, Xu S, Itohara S, Tonegawa S. Antagonistic negative and positive neurons of the basolateral amygdala. *Nat Neurosci*. 2016;19:1636–46. <https://doi.org/10.1038/nn.4414>.
20. Wesson DW. The tubular striatum. *J Neurosci*. 2020;40:7379–86.
21. Nishi A, Snyder GL, Greengard P. Bidirectional regulation of DARPP-32 phosphorylation by dopamine. *J Neurosci*. 1997;17:8147 LP–8155. <http://www.jneurosci.org/content/17/21/8147.abstract>.
22. Svenningsson P, Nishi A, Fisone G, Girault JA, Nairn AC, Greengard P. DARPP-32: an integrator of neurotransmission. *Annu Rev Pharmacol Toxicol*. 2004;44:269.
23. Ouimet CC, Miller PE, Hemmings HC, Walaas SI, Greengard P. DARPP-32, a dopamine- and adenosine 3':5'-monophosphate-regulated phosphoprotein enriched in dopamine-innervated brain regions. III. Immunocytochemical localization. *J Neurosci*. 1984;4:111–24.
24. Scibilia RJ, Lachowicz JE, Kilts CD. Topographic nonoverlapping distribution of D1 and D2 dopamine receptors in the amygdaloid nuclear complex of the rat brain. *Synapse*. 1992;11:146–54.
25. Fadok JP, Dickerson TMK, Palmiter RD. Dopamine is necessary for cue-dependent fear conditioning. *J Neurosci*. 2009;29:11089–97.
26. Zhang X, Kim J, Tonegawa S. Amygdala reward neurons form and store fear extinction memory. *Neuron*. 2020;105:1077–93.e7. <https://www.sciencedirect.com/science/article/pii/S0896627319310918>.
27. Guarraci FA, Frohardt RJ, Falls WA, Kapp BS. The effects of intra-amygdaloid infusions of a D₂ dopamine receptor antagonist on pavlovian fear conditioning. *Behav Neurosci*. 2000;114:647–51.
28. de Oliveira AR, Reimer AE, de Macedo CE, de Carvalho MC, Silva MA, Brandão ML. Conditioned fear is modulated by D2 receptor pathway connecting the ventral tegmental area and basolateral amygdala. *Neurobiol Learn Mem*. 2011;95:37–45. <https://www.sciencedirect.com/science/article/pii/S1074742710001723>.
29. Berglind WJ, Case JM, Parker MP, Fuchs RA, See RE. Dopamine D1 or D2 receptor antagonism within the basolateral amygdala differentially alters the acquisition of cocaine-cue associations necessary for cue-induced reinstatement of cocaine-seeking. *Neuroscience*. 2006;137:699–706.
30. Gong S, Zheng C, Doughty ML, Losos K, Didkovsky N, Schambra UB, et al. A gene expression atlas of the central nervous system based on bacterial artificial chromosomes. *Nature*. 2003;425:917–25. http://www.ncbi.nlm.nih.gov/entrez/query.fcgi?cmd=Retrieve&db=PubMed&dopt=Citation&list_uids=14586460.
31. Shuen JA, Chen M, Gloss B, Calakos N. Drd1a-tdTomato BAC transgenic mice for simultaneous visualization of medium spiny neurons in the direct and indirect pathways of the basal ganglia. *J Neurosci*. 2008;28:2681–5. <https://doi.org/10.1523/JNEUROSCI.5492-07.2008>.
32. Madisen L, Zwingman TA, Sunkin SM, Oh SW, Zariwala HA, Gu H, et al. A robust and high-throughput Cre reporting and characterization system for the whole mouse brain. *Nat Neurosci*. 2010;13:133–40. <http://www.ncbi.nlm.nih.gov/pmc/articles/PMC2840225/>.
33. Herman AM, Ortiz-Guzman J, Kochukov M, Herman I, Quast KB, Patel JM, et al. A cholinergic basal forebrain feeding circuit modulates appetite suppression. *Nature*. 2016;538:253–6. <https://doi.org/10.1038/nature19789>.
34. Paxinos G, Franklin K. The mouse brain in stereotaxic coordinates. 2nd ed. San Diego: Academic Press; 2000.
35. Bonaventura J, Eldridge MAG, Hu F, Gomez JL, Sanchez-Soto M, Abramyan AM, et al. High-potency ligands for DREADD imaging and activation in rodents and monkeys. *Nat Commun*. 2019;10:4627. <https://doi.org/10.1038/s41467-019-12236-z>.
36. Hegoburu C, Shionoya K, Garcia S, Messaoudi B, Thévenet M, Mouly A-M. The RUB cage: respiration–ultrasonic vocalizations–behavior acquisition setup for assessing emotional memory in rats. *Front Behav Neurosci*. 2011;5:25. http://www.frontiersin.org/Journal/Abstract.aspx?s=99&name=behavioral_neuroscience&ART_DOI=10.3389/fnbeh.2011.00025.
37. Gadziola MA, Tylicki KA, Christian DL, Wesson DW. The olfactory tubercle encodes odor valence in behaving mice. *J Neurosci*. 2015;35:4515–27. <http://www.jneurosci.org/content/35/11/4515.abstract>.
38. Johnson ME, Bergkvist L, Mercado G, Stetzk L, Meyerdirk L, Wolfrum E, et al. Deficits in olfactory sensitivity in a mouse model of Parkinson's disease revealed by plethysmography of odor-evoked sniffing. *Sci Rep*. 2020;10:9242. <https://www.nature.com/articles/s41598-020-66201-8>.
39. Pennington ZT, Dong Z, Feng Y, Vetere LM, Page-Harley L, Shuman T, et al. ezTrack: an open-source video analysis pipeline for the investigation of animal behavior. *Sci Rep*. 2019;9:19979. <https://doi.org/10.1038/s41598-019-56408-9>.
40. Wei X, Ma T, Cheng Y, Huang CCY, Wang X, Lu J, et al. Dopamine D1 or D2 receptor-expressing neurons in the central nervous system. *Addict Biol*. 2018;23:569–84.
41. Gong S, Doughty M, Harbaugh CR, Cummins A, Hatten ME, Heintz N, et al. Targeting cre recombinase to specific neuron populations with bacterial artificial chromosome constructs. *J Neurosci*. 2007;27:9817 LP–9823. <http://www.jneurosci.org/content/27/37/9817.abstract>.
42. Rebola N, Canas PM, Oliveira CR, Cunha RA. Different synaptic and subsynaptic localization of adenosine A2A receptors in the hippocampus and striatum of the rat. *Neuroscience*. 2005;132:893–903.
43. Li W, Howard JD, Parrish TB, Gottfried JA. Aversive learning enhances perceptual and cortical discrimination of indiscriminable odor cues. *Science*. 2008;319:1842–5. http://www.ncbi.nlm.nih.gov/entrez/query.fcgi?cmd=Retrieve&db=PubMed&dopt=Citation&list_uids=18369149.
44. Wilson DA, Sullivan RM. Cortical processing of odor objects. *Neuron*. 2011;72:506–19.
45. White KA, Zhang Y-F, Zhang Z, Bhattarai JP, Moberly AH, in 't Zandt E, et al. Glutamatergic neurons in the piriform cortex influence the activity of D1 and D2-type receptor expressing olfactory tubercle neurons. *J Neurosci*. 2019;38:9546–59. <http://www.ncbi.nlm.nih.gov/pubmed/31628176>.
46. Best AR, Wilson DA. A postnatal sensitive period for plasticity of cortical afferents but not cortical association fibers in rat piriform cortex. *Brain Res*. 2003;961:81–7. http://www.ncbi.nlm.nih.gov/entrez/query.fcgi?cmd=Retrieve&db=PubMed&dopt=Citation&list_uids=12535779.
47. Jones SV, Choi DC, Davis M, Ressler KJ. Learning-dependent structural plasticity in the adult olfactory pathway. *J Neurosci*. 2008;28:13106 LP–13111. <http://www.jneurosci.org/content/28/49/13106.abstract>.
48. Moberly AH, Schreck M, Bhattarai JP, Zweifel LS, Luo W, Ma M. Olfactory inputs modulate respiration-related rhythmic activity in the prefrontal cortex and freezing behavior. *Nat Commun*. 2018;9:1528. <https://doi.org/10.1038/s41467-018-03988-1>.

49. Cardinal RN, Parkinson JA, Hall J, Everitt BJ. Emotion and motivation: the role of the amygdala, ventral striatum, and prefrontal cortex. *Neurosci Biobehav Rev*. 2002;26:321–52. http://www.ncbi.nlm.nih.gov/entrez/query.fcgi?cmd=Retrieve&db=PubMed&dopt=Citation&list_uids=12034134.
50. Paré D, Quirk GJ, Ledoux JE. New vistas on amygdala networks in conditioned fear. *J Neurophysiol*. 2004;92:1–9. <http://jn.physiology.org/content/92/1/1.abstract>.
51. Ambroggi F, Ishikawa A, Fields HL, Nicola SM. Basolateral amygdala neurons facilitate reward-seeking behavior by exciting nucleus accumbens neurons. *Neuron*. 2008;59:648–61.
52. Stuber GD, Sparta DR, Stamatakis AM, van Leeuwen WA, Hardjoprajitno JE, Cho S, et al. Excitatory transmission from the amygdala to nucleus accumbens facilitates reward seeking. *Nature*. 2011;475:377. <https://doi.org/10.1038/nature10194>.
53. Janak PH, Tye KM. From circuits to behaviour in the amygdala. *Nature*. 2015;517:284. <https://doi.org/10.1038/nature14188>.
54. Beyeler A, Namburi P, Glover GF, Simonnet C, Calhoun GG, Conyers GF, et al. Divergent routing of positive and negative information from the amygdala during memory retrieval. *Neuron*. 2016;90:348–61. <https://www.sciencedirect.com/science/article/pii/S0896627316001835>.
55. Meador-Woodruff JH, Mansour A, Healy DJ, Kuehn R, Zhou QY, Bunzow JR, et al. Comparison of the distributions of D1 and D2 dopamine receptor mRNAs in rat brain. *Neuropsychopharmacology*. 1991;5:231–42.
56. West EA, Carelli RM. Nucleus accumbens core and shell differentially encode reward-associated cues after reinforcer devaluation. *J Neurosci*. 2016;36:1128–39. <http://www.jneurosci.org/content/36/4/1128.abstract>.
57. Zhang Z, Liu Q, Wen P, Zhang J, Rao X, Zhou Z, et al. Activation of the dopaminergic pathway from VTA to the medial olfactory tubercle generates odor-preference and reward. *eLife*. 2017;6:e25423.
58. Murata K, Kanno M, Ieki N, Mori K, Yamaguchi M. Mapping of learned odor-induced motivated behaviors in the mouse olfactory tubercle. *J Neurosci*. 2015;35:10581–99. <http://www.jneurosci.org/content/35/29/10581.abstract>.
59. Stevenson I, Ripley HS. Variations in respiration and in respiratory symptoms during changes in emotion. *Psychosom Med*. 1952;14:476–90.
60. Boiten FA. The effects of emotional behaviour on components of the respiratory cycle. *Biol Psychol*. 1998;49:29–51.
61. Homma I, Masaoka Y. Breathing rhythms and emotions. *Exp Physiol*. 2008;93:1011–21.
62. Walker P, Carrive P. Role of ventrolateral periaqueductal gray neurons in the behavioral and cardiovascular responses to contextual conditioned fear and poststress recovery. *Neuroscience*. 2003;116:897–912. <http://www.sciencedirect.com/science/article/pii/S0306452202007443>.
63. Subramanian HH, Holstege G. Stimulation of the midbrain periaqueductal gray modulates preinspiratory neurons in the ventrolateral medulla in the rat in vivo. *J Comp Neurol*. 2013;521:3083–98. <https://onlinelibrary.wiley.com/doi/10.1002/cne.23334>.
64. Lamont EW, Kokkinidis L. Infusion of the dopamine D1 receptor antagonist SCH 23390 into the amygdala blocks fear expression in a potentiated startle paradigm. *Brain Res*. 1998;795:128–36. <https://www.sciencedirect.com/science/article/pii/S0006899398002819>.
65. Greba Q, Giffkins A, Kokkinidis L. Inhibition of amygdaloid dopamine D2 receptors impairs emotional learning measured with fear-potentiated startle. *Brain Res*. 2001;899:218–26. <https://www.sciencedirect.com/science/article/pii/S0006899301022430>.
66. Shionoya K, Hegoburu C, Brown B, Sullivan R, Doyère V, Mouly A-M. It's time to fear! interval timing in odor fear conditioning in rats [Internet]. *Front Behav Neurosci*. 2013;7:128. <https://www.frontiersin.org/articles/10.3389/fnbeh.2013.00128>.
67. de Souza Caetano KA, de Oliveira AR, Brandão ML. Dopamine D2 receptors modulate the expression of contextual conditioned fear: role of the ventral tegmental area and the basolateral amygdala. *Behav Pharmacol*. 2013;24:264–74. https://journals.lww.com/behaviouralpharm/Fulltext/2013/08000/Dopamine_D2_receptors_modulate_the_expression_of.4.aspx.
68. See RE, Kruzich PJ, Grimm JW. Dopamine, but not glutamate, receptor blockade in the basolateral amygdala attenuates conditioned reward in a rat model of relapse to cocaine-seeking behavior. *Psychopharmacology (Berl)*. 2001;154:301–10.
69. Kim ES, Lattal KM. Context-dependent and context-independent effects of D1 receptor antagonism in the basolateral and central amygdala during cocaine self-administration. *eNeuro*. 2019;6:ENEURO.0203–19.2019.
70. Kröner S, Rosenkranz JA, Grace AA, Barrionuevo G. Dopamine modulates excitability of basolateral amygdala neurons in vitro. *J Neurophysiol*. 2005;93:1598–610. <https://doi.org/10.1152/jn.00843.2004>.
71. Richfield EK, Penney JB, Young AB. Anatomical and affinity state comparisons between dopamine D1 and D2 receptors in the rat central nervous system. *Neuroscience*. 1989;30:767–77. <https://www.sciencedirect.com/science/article/pii/0306452289901681>.
72. Schultz W. Multiple DA functions at different time courses. *Annu Rev Neurosci*. 2007;30:259.
73. Horvitz JC. Mesolimbocortical and nigrostriatal dopamine responses to salient non-reward events. *Neuroscience*. 2000;96:651–6. <https://www.sciencedirect.com/science/article/pii/S0306452200000191>.
74. Guarraci FA, Frohardt RJ, Young SL, Kapp BS. A functional role for dopamine transmission in the amygdala during conditioned fear. *Ann N Y Acad Sci*. 1999;877:732–6. <https://doi.org/10.1111/j.1749-6632.1999.tb09312.x>.
75. Bristol AS, Sutton MA, Carew TJ. Neural circuit of tail-elicited siphon withdrawal in *Aplysia*. I. Differential lateralization of sensitization and dishabituation. *J Neurophysiol*. 2004;91:666–77. http://www.ncbi.nlm.nih.gov/entrez/query.fcgi?cmd=Retrieve&db=PubMed&dopt=Citation&list_uids=13679401.
76. Tian Z, Song J, Zhao X, Zhou Y, Chen X, Le Q, et al. The interhemispheric amygdala-accumbens circuit encodes negative valence in mice. *Science*. 2024;386:eadp7520. <https://doi.org/10.1126/science.adp7520>.
77. Fleming LL, Harnett NG, Ressler KJ. Sensory alterations in post-traumatic stress disorder. *Curr Opin Neurobiol*. 2024;84:102821. <https://www.sciencedirect.com/science/article/pii/S0959438823001460>.

ACKNOWLEDGEMENTS

We thank Dr. Marc Fuccillo for generously sharing reagents for synaptophysin-based AAV tracing. This work was supported by R01DC014443 and R01DC016519 to D.W.W., and R01DA049545 to D.W.W. and M.M.. N.L.J. was supported by NIDCD T32015994 and F31DC020364. J.B. was supported by R21DC019193. S.E.S. was supported by T32DC015994 and F31DC021888.

AUTHOR CONTRIBUTIONS

Conceptualization: SER, SES, DWW. Methodology: NLJ, ERT, EJ, AAC. Investigation: SES, SER, MMK, JB, YW, GMS, SRI, YFZ, MM, DWW. Visualization: SER, SES, DWW. Funding acquisition: DWW, NLJ, SES, MM. Supervision: DWW, MM. Writing – original draft: SES, SER, DWW. Writing – review & editing: SES, SER, MMK, SRI, DWW, MM. MMK, JB, and YW contributed equally to this work.

COMPETING INTERESTS

The authors declare no competing interests.

ADDITIONAL INFORMATION

Supplementary information The online version contains supplementary material available at <https://doi.org/10.1038/s41380-025-03075-0>.

Correspondence and requests for materials should be addressed to Daniel W. Wesson.

Reprints and permission information is available at <http://www.nature.com/reprints>

Publisher's note Springer Nature remains neutral with regard to jurisdictional claims in published maps and institutional affiliations.



Open Access This article is licensed under a Creative Commons Attribution-NonCommercial-NoDerivatives 4.0 International License, which permits any non-commercial use, sharing, distribution and reproduction in any medium or format, as long as you give appropriate credit to the original author(s) and the source, provide a link to the Creative Commons licence, and indicate if you modified the licensed material. You do not have permission under this licence to share adapted material derived from this article or parts of it. The images or other third party material in this article are included in the article's Creative Commons licence, unless indicated otherwise in a credit line to the material. If material is not included in the article's Creative Commons licence and your intended use is not permitted by statutory regulation or exceeds the permitted use, you will need to obtain permission directly from the copyright holder. To view a copy of this licence, visit <http://creativecommons.org/licenses/by-nc-nd/4.0/>.

© The Author(s) 2025